Evaluation of the anti-biofilm activities of bacterial cellulose-tannic acid-magnesium chloride composites using an *in vitro* multispecies biofilm model

Wei He[a,b,1], Zhaoyu Zhang[a,1], Jing Chen[a,1], Yudong Zheng[a*], Yajie Xie[a], Wenbo Liu[a,c], Jian Wu[b,d,e], Dina A. Mosselhy[f,g]

[a]School of Materials Science and Engineering, University of Science and Technology Beijing, Beijing 100083, China

[b]Suzhou Xiangcheng Medical Materials Science and Technology Co., Ltd., Suzhou 215028, China

[c]Center for Medical Device Evaluation, National Medical Products Administration, Beijing, China

[d]Advanced Materials Division, Suzhou Institute of Nano-Tech and Nano-Bionics, Chinese Academy of Sciences, Suzhou 215123, China

[e]Division of Nanomaterials, Suzhou Institute of Nano-Tech and Nano-Bionics, Chinese Academy of Sciences, Nanchang 330200, China

[f]Department of Virology, Faculty of Medicine, University of Helsinki, P.O. Box 21, 00014 Helsinki, Finland

[g]Department of Veterinary Biosciences, Faculty of Veterinary Medicine, University of Helsinki, P.O. Box 66, 00014 Helsinki, Finland

[1] The first three authors contributed equally to this manuscript.

* Corresponding author: Yudong Zheng

Email: zhengyudong@mater.ustb.edu.cn

Address: 30 Xueyuan Road, Haidian District, Beijing, China.

Tel: +86-10-62330802; Fax: 86-10-62332336

© The Author(s) 2020. Published by Oxford University Press.
This is an Open Access article distributed under the terms of the Creative Commons Attribution License (http://creativecommons.org/licenses/by/4.0/), which permits unrestricted reuse, distribution, and reproduction in any medium, provided the original work is properly cited.

Downloaded from https://academic.oup.com/rb/advance-article/doi/10.1093/rb/rbab054/6381593 by Viikki Science Library user on 07 October 2021

Abstract

Chronic wounds are a serious worldwide problem, which are often accompanied by wound infections. In this study, bacterial cellulose (BC)-based composites introduced with tannic acid (TA) and magnesium chloride (BC-TA-Mg) were fabricated for anti-biofilm activities. The prepared composites' surface properties, mechanical capacity, thermal stability, water absorption and retention property, releasing behavior, anti-biofilm activities, and potential cytotoxicity were tested. Results show that TA and $MgCl_2$ particles closely adhered to the nanofibers of BC membranes, thus increasing surface roughness and hydrophobicity of the membranes. While the introduction of TA and $MgCl_2$ did not influence the transparency of the membranes, making it beneficial for wound inspection. BC-TA and BC-TA-Mg composites displayed increased tensile strength and elongation at break compared to pure BC. Moreover, BC-TA-Mg exhibited higher water absorption and retention capacity than BC and BC-TA, suitable for the absorption of wound exudates. BC-TA-Mg demonstrated controlled release of TA and good inhibitory effect on both singly-cultured *S. aureus* and *P. aeruginosa* biofilm and co-cultured biofilm of *S. aureus* and *P. aeruginosa*. Furthermore, the cytotoxicity grade of BC-TA-6Mg membrane was eligible based on standard toxicity classifications. These indicated that BC-TA-Mg is potential to be used as wound dressings combating biofilms in chronic wounds.

Keywords: bacterial cellulose; tannic acid; magnesium chloride; anti-biofilm activities

1. Introduction

Chronic wounds are a serious worldwide problem, which bring a heavy burden to the

Downloaded from https://academic.oup.com/rb/advance-article/doi/10.1093/rb/rbab054/6381593 by Viikki Science Library user on 07 October 2021

patient and healthcare system. The wound is considered a chronic wound when the healing period is one month or more [1]. Chronic wounds mainly include diabetic foot ulcers, bedsores or pressure sores, venous leg ulcers, and nonhealing surgical site infections [2, 3]. In China, it has been shown that the leading cause of chronic wounds was diabetes [3]. In Europe, over 55 million patients suffering from diabetes, and 8 million of them may develop a diabetic foot ulcer. What's worse, if the patients got poor treatment, they would progress to lower limb amputation [4]. Infection and inadequate blood supply to blood vessels can lead to chronic wounds. Infection is caused by microbial reproduction in the wound bed, resulting in prolonged inflammatory response, delayed collagen synthesis and epithelial formation, thus damaging the skin tissue [5]. Chronic infection is a persistent and progressive pathology mainly caused by inflammation around the biofilm in the body [6]. It was found that the prevalence of biofilms in acute wounds was only 6% [7], while as many as 78.2% of chronic wounds contained biofilms [8]. *Enterococcus faecium*, *Staphylococcus aureus*, *Klebsiella pneumoniae*, *Acinetobacter baumannii*, *Pseudomonas aeruginosa* and *Enterobacter species.* (i.e., ESKAPE pathogens) have been shown to be the key pathogens involved in chronic wounds infections and biofilms [9-11]. There is a consensus in the wound care community that among most wound infections, bacteria attach to wound surfaces and proliferate in the infected wound, delaying healing [12] and causing failure of treatment of wound infections [2]. Biofilms are intricate bacterial aggregates, producing an extracellular polymeric substance (EPS, a three-dimensional physical matrix formed of exopolysaccharides, lipids, proteins, and extracellular

Downloaded from https://academic.oup.com/rb/advance-article/doi/10.1093/rb/rbab054/6381593 by Viikki Science Library user on 07 October 2021

deoxyribonucleic acid, empowering bacteria with excessive resistance or tolerance against antibiotics) [13]. EPS encloses the cells, adheres to wounds, and prevents the penetration of antibiotics [9, 11].

Therefore, there is an urgent demand for novel therapeutic strategies that can defeat the bacteria and their biofilms in chronic wound infections. Bacterial cellulose (BC) is a natural polymer secreted by certain bacteria [14]. It has many unique physical, chemical, and biological properties, such as ultrafine nanofiber network, high tensile strength and elastic modulus, high water absorption and retention capacity, high crystallinity, and good biocompatibility [14, 15]. BC-based wound dressings functionalized with different antibacterial agents have been proved to be ideal materials for dealing with chronic wound infections. For example, Picolotto *et al.* [16] synthesized BC/red propolis composite and utilized the composite to treat diabetic mice wounds. *In vivo* experiments revealed that BC/red propolis accelerated wound healing of diabetic mice by inducing a decreased lesion size, less inflammation, an increase of TGF-β levels, and complete epithelization. Liu *et al.* [17] chemically anchored BC with quaternary ammonium salt through 2-methacryloyloxyethyl trimethylammonium chloride. The composite membrane displayed good antibacterial activities against *S. aureus* and *Escherichia coli*, and it improved healing of mouse wounds infected with *E. coli*. Wu *et al.* [18, 19] produced BC/silver nanoparticles composite, and the composite showed strong antibacterial activities. Moreover, in comparison with BC and blank control, it induced less inflammation and promoted burn wound healing in dealing with a second-degree rat scald wound. However, none of the above studies evaluated the anti-biofilm

Downloaded from https://academic.oup.com/rb/advance-article/doi/10.1093/rb/rbab054/6381593 by Viikki Science Library user on 07 October 2021

activities of the prepared materials.

In our previous work, BC-based membranes incorporated with tannic acid (TA) and magnesium chloride (BC-TA-Mg) were prepared for the purposes of antimicrobial and anti-biofilm [20]. TA is an excellent inhibitor against various bacteria [21], which could also inhibit *S. aureus* and *P. aeruginosa* biofilm formation[22]. The composites displayed a controlled-release of TA, depending on the incorporated Mg^{2+} concentration. The released rate of TA was decreased through introducing more Mg^{2+} into the composites, resulting in lower cytotoxicity to L929. The BC-TA-Mg composites demonstrated intense antibacterial activities against *S. aureus*, *P. aeruginosa*, and *E. coli* and excellent inhibition on *S. aureus* and *P. aeruginosa* biofilm formation. In our previous work, microtiter plate method was used to test the effects of the BC-TA-Mg composites on the formation of singly-cultured *S. aureus* and *P. aeruginosa* biofilms [20]. However, the chronic wound environment is complex and rich in nutrients, and chronic wound infection is often associated with varieties of bacteria, both gram-positive and gram-negative species [10, 11, 23]. Therefore, it will be more meaningful to test the effects of the materials on biofilm formation of co-cultured gram-positive and gram-negative bacteria systems, which is closer to a real wound environment. To achieve this, a model that can simultaneously support the growth of gram-positive and gram-negative bacteria species should be applied. Moreover, as discussed above, the material was utilized as a wound dressing to deal with chronic wounds. It will be ideal to build an *in vitro* artificial wound bed model to test the effects of wound dressings on biofilm formation, which is particularly important

Downloaded from https://academic.oup.com/rb/advance-article/doi/10.1093/rb/rbab054/6381593 by Viikki Science Library user on 07 October 2021

for the early-stage research and development of wound dressings. Some studies reported the development of multispecies biofilm models. However, relatively few studies reported applying *in vitro* models in testing the inhibitory effects of wound dressings or some other materials on biofilm formation. Hammond *et al.* [24] inoculated cellulose discs with burn wound bacterial isolates (*S. aureus* and *P. aeruginosa*) and then placed them on agar plates. After incubation for 24 h, a burn wound biofilm model was established. The model was then covered with antibiotic ointments-soaked gauze to check the influence of antibiotic ointments on biofilm formation. Kucera *et al.* [25] employed a famous "Lubbock chronic wound biofilm (LCWB) model" [26] to establish multispecies (i.e., *S. aureus*, *E. faecalis*, *Bacillus subtilis*, and *P. aeruginosa*) biofilm and then moved the prepared biofilm onto an artificial wound bed. They demonstrated that this model was applicable to novel therapeutics intended for combating chronic wound biofilms.

In this study, BC-TA-Mg composites were fabricated, and surface properties, mechanical capacity, thermal stability, water absorption and retention property, releasing behavior of the prepared composites membranes were tested. Thereafter, a modified LCWB model was used to develop a multispecies biofilm, and then the biofilm was moved onto an artificial wound bed. BC-TA-Mg composites were covered on biofilm to evaluate its anti-biofilm activities. Gram staining, FITC-ConA staining, and plate colony-counting method were conducted to assess the effect of BC-TA-Mg composites on the formation of biofilm of co-cultured *S. aureus* and *P. aeruginosa*. Finally, the potential cytotoxicity of prepared composites was detected. Results

Downloaded from https://academic.oup.com/rb/advance-article/doi/10.1093/rb/rbab054/6381593 by Viikki Science Library user on 07 October 2021

demonstrated that the composites were transparent and exhibited improved mechanical properties, water absorption and retention capacity compared with pure BC. Moreover, they displayed potent anti-biofilm activities, suggesting that they are potential to be used as wound dressings to treat chronic wounds. Fig. 1 described the anti-biofilm activities of BC-TA-Mg composites and the anti-biofilm tests performed in this study.

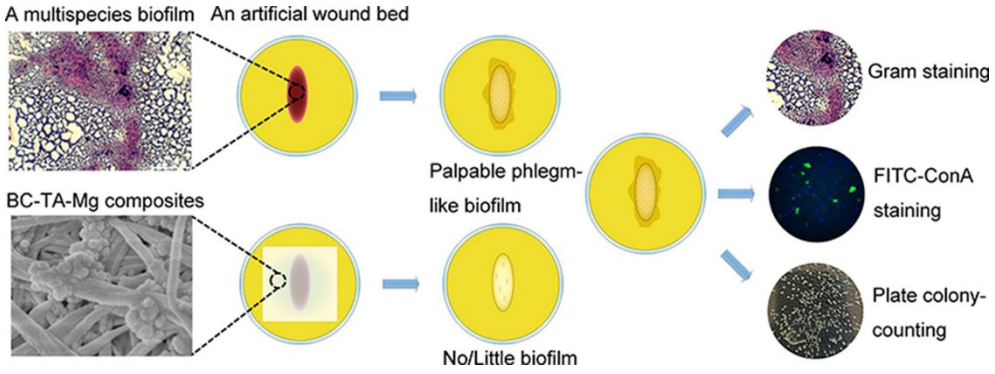

Fig. 1 Schematic illustration of the anti-biofilm activities of BC-TA-Mg composites and the related tests performed in this study.

2. Materials and Methods

2.1 Preparation and Characterization of BC-TA-Mg composites

BC membranes, with a thickness of 3 mm and a state of hydrogel, were acquired from Hainan Yida Food Co. Ltd. (Hainan, China). BC-TA-Mg composites were prepared using the same method described in our previous work [20]. In brief, BC was first purified to remove impurities using the same approach as He *et al*. [27]. After purification, BC was cut into round pieces (diameter of 10 mm) and immersed in 15 mL 4 mM TA solution. Thereafter, 15 mL $MgCl_2$ solution in 4, 8 or 12 mM was added to the TA solution. Subsequently, 1 M NaOH solution was dropped into the mixture to

Downloaded from https://academic.oup.com/rb/advance-article/doi/10.1093/rb/rbab054/6381593 by Viikki Science Library user on 07 October 2021

adjust the pH to 6. The mixture was stirred for 10 min, and then BC-TA-Mg composites were obtained after the mixture was kept for 24 h. For BC-TA composite, no $MgCl_2$ or NaOH solution was added.

Scanning electron microscope (SEM) was used to observe the surface morphology of BC and composite materials. Wet membranes were freeze-dried, coated with carbon layers, and then observed under SEM (Hitachi SU8020, Japan). The distribution of Mg element on the surface of the membranes was determined by an electron microprobe analyzer (EMPA, JXA-8230, JEOL, Japan).

The amount of TA loaded to BC was determined by the following formula:

Weight of TA = $W_1 - W_2$

Where W_1 and W_2 were the amounts of TA before and after BC was immersed in TA solution. W_2 was measured by UV spectrophotometry. In brief, the TA solution was collected after BC membranes were taken out from the solution. The samples were washed thrice with distilled water, and the cleaning solution was also collected. TA solution and cleaning solution were mixed together, and then the absorbance at 276 nm of the mixture was tested under a UV-VIS spectrophotometer. The amount of TA contained in the mixture (W_2) was determined by comparing the absorbance to the standard curve. Furthermore, the quantitative amount of Mg element contained in BC-TA-Mg composites was tested by inductively coupled plasma mass spectrometry (ICP-MS, Agilent 7500ce, USA).

The elemental composition of samples was analyzed by X-ray photoelectron spectroscopy (XPS, ESCALAB 250Xi, Thermo Scientific, USA). The survey scan of

Downloaded from https://academic.oup.com/rb/advance-article/doi/10.1093/rb/rbab054/6381593 by Viikki Science Library user on 07 October 2021

BC, BC-TA, and BC-TA-6Mg and high-resolution scan of Mg 2p of BC-TA-6Mg were recorded. Aliphatic carbon (C 1 s = 284.8 eV) was used to calibrate all binding energies. Atomic force microscope (AFM, Bruker, USA) was utilized to test surface topography of the air-dried samples with a scanned area of 5.0 μm × 5.0 μm. The water contact angle of the air-dried membranes was tested using a contact angle meter (OCA20, Dataphysics Inc., Germany). The membranes were also recorded by a TENSOR II Fourier transform infrared spectroscopy (FTIR) (Bruker, German). A thermal analyzer (SDT Q600, TA Instruments, USA) was applied to measure the thermal properties of air-dried membranes. Membranes were heated from 30 °C to 585 °C in nitrogen. Tensile stress-strain properties of wet membranes were tested under a Stable Micro Systems TAHD plus Texture Analyzer. Membranes were cut into dumbbell shapes consisting with ASTM D 638-2003 Type IV specimens.

The water absorption of air-dried membranes was measured using a gravimetric method [28]. The initial dry weights of the membranes (W_0) were tested. Thereafter, membranes were dipped into deionized water (with a pH of 5 and 8 adjusted by HCl and NaOH, respectively) and then kept at 37°C. After some time, the weights of membranes (Wi) were tested after water on surfaces was removed. Water absorption was determined as follows:

Water absorption= $(W_i-W_0)/W_0 \times 100\%$

The water retention capacity of the membranes was also tested according to our previous report [28]. The initial weights of dry membranes were measured (W_0). Afterward, the samples were dipped into deionized water and then kept at 37°C for 24

Downloaded from https://academic.oup.com/rb/advance-article/doi/10.1093/rb/rbab054/6381593 by Viikki Science Library user on 07 October 2021

h. Subsequently, water on surfaces of membranes was absorbed, and then membranes were put into centrifuge tubes. After centrifuging for 3 min (500 r/min), the weights of membranes were measured again (W_1). The water retention capacity was determined by the following equation:

Water retention = $(W_1-W_0)/W_0 \times 100\%$

The releasing behavior of TA from BC-TA and BC-TA-Mg composites was monitored by UV spectrophotometry. Membranes were placed in a 24-well plate, and 2 mL PBS was added to each well. The samples were then put into an incubator at 37 ℃. After 2 h, for each sample, supernatant PBS was collected, and then 2 mL fresh PBS were added. The same operations were repeated, and supernatants at fixed intervals were obtained. The absorbance at 276 nm of the collected supernatant was measured under an UV-VIS spectrophotometer. By comparing the absorbance to that of the standard curve, the release of TA was determined. The cumulative release of TA was determined by the superposition principle.

2.2 Establishment of *In vitro* multispecies biofilm model

S. aureus (ATCC 23923) and *P. aeruginosa* (ATCC 27853) were obtained from the American Type Culture Collection. They were maintained in sterilized TSB medium and modified M9 medium for 24 h, respectively. Afterward, the medium was diluted to achieve a 1×10^6 CFU/mL bacterial concentration, thus obtaining the standard bacterial suspension. *In vitro* chronic wound biofilm was obtained by adopting a modified LCWB method according to Sun *et al.* [26]. In brief, 6 mL medium containing 45% TSB medium, 50% bovine plasma, and 5% lysed horse blood was added into a

Downloaded from https://academic.oup.com/rb/advance-article/doi/10.1093/rb/rbab054/6381593 by Viikki Science Library user on 07 October 2021

polystyrene test tube. Then, 10 μL standard bacterial suspension was inoculated into the medium. The bacteria were incubated at 37 ℃ with shaking (150 r/min) for 48 h.

2.3 Establishment of a biofilm on an artificial wound bed

An artificial wound bed was established according to a previous report [25]. The sterilized LB medium was poured into the petri dish to obtain a thickness of 2 mm. After the medium was solidified, a sterilized 20 mm × 8 mm polytetrafluoroethylene-coated magnetic stir bar was placed in the center of the petri dish. Then the second layer of LB medium was added, and its thickness was kept 2 mm. After the medium was completely solidified, the magnetic stir bar was carefully removed from the agar medium, resulting in an oval artificial wound bed. The preformed mature biofilm was moved with a pipette and then placed on an artificial wound bed in LB solid medium. Finally, the artificial wound bed was covered with a piece of BC-TA-Mg composite. The artificial wound bed was incubated at 37 ℃ for 24 hours. The group without covering was used as a control. After that, the biofilm was photographed and then carefully collected with a sterilized forcep and a dipper. The collected biofilm was homogenized and then used for staining and quantification of bacteria amount.

2.4 SEM observation of biofilm

The biofilm of the control group was collected for SEM observation. In brief, biofilm was rinsed with PBS and then fixed in 2.5% glutaraldehyde. Afterward, it was immersed in a series of graded ethanol (30, 50, 75, 85, 95, and 100 v/v%) for dehydration. After that, the biofilm was treated with a series of tertiary butyl alcohol (25, 50, 75, and 100 v/v%) for solvent replacement. At last, it was freeze-dried,

Downloaded from https://academic.oup.com/rb/advance-article/doi/10.1093/rb/rbab054/6381593 by Viikki Science Library user on 07 October 2021

sputtered with platinum, and then observed by SEM (GeminiSEM 300, ZEISS, Germany).

2.5 Gram staining

Briefly, a drop of sterilized water was dropped on a sterilized glass slide. Then, 10 μL bacterial biofilm was added and mixed with the water droplet on the glass slide using a pipette, forming a bacterial suspension. Therefore, the glass slide was coated with a thin layer of bacterial suspension and dried in air. Afterward, the glass slide was passed through the outer layer of the flame of the alcohol lamp 3 times, and the glass slide was kept on the flame for 2 to 3 seconds each time for fixation. Biofilm was stained by immersing the glass slide in 2% crystal violet for 1 min. Subsequently, the sample was rinsed with sterilized water several times and then observed under an optical microscope (DYF 800, Dianying Optics, China). The stained area of each sample was quantified based on the image data using the software Image-Pro Plus Vision 6.0. The reduction rate of biofilms was calculated as the following:

Reduction rate of biofilms = $(m_0 - m_1)/m_0 \times 100\%$

where m_0 and m_1 are the amount of stained biofilms of the control and experimental group, respectively.

2.6 FITC-ConA staining

Samples were prepared, dried, and fixed as described above. After that, bacteria were fixed with paraformaldehyde (4% (w/v)), washed thrice with PBS, and then dried in air. Subsequently, they were stained with 50 μg/mL FITC-ConA (Invitrogen, USA) and 1 μg/mL DAPI. After being washed thrice with PBS, samples were observed under an

Downloaded from https://academic.oup.com/rb/advance-article/doi/10.1093/rb/rbab054/6381593 by Viikki Science Library user on 07 October 2021

inverted fluorescence microscope (Zeiss, Germany). The intergraded optical density of polysaccharides and nuclei was quantified based on the image data using the software Image-Pro Plus Vision 6.0. The reduction rate of intergraded optical density was calculated as the following:

Reduction rate of intergraded optical density = $(n_0 - n_1)/n_0 \times 100\%$

where n_0 and n_1 are the amount of intergraded optical density of the control and experimental group, respectively.

2.7 Plate colony-counting method

10 μL bacterial biofilm was taken by using a pipette and placed in a sterilized centrifuge tube. 1 mL TSB medium was added into each tube, and the bacterial suspension was ultrasonically shaken for 5 min to make the bacteria evenly dispersed. The homogenized bacterial suspension was then diluted with TSB medium in a ratio of 1:10,000. Then 100 μL diluted bacterial suspension was re-inoculated in LB agar medium (for cocultured biofilm, the medium contains particular inhibitors for *S. aureus* or *P. aeruginosa*). After incubation for 24 h, images were taken to record the number of colonies. Finally, the number of bacteria per unit volume (CFU/mL) was calculated.

2.8 *In vitro* cytotoxicity tests of BC-TA-Mg composites

The possible cytotoxicity of BC-TA-Mg composites on human embryonic dermal fibroblasts (CCC-ESF-1) was evaluated *in vitro*. Cells were purchased from the China Infrastructure of Cell Life Source. They were kept in high-glucose Dulbecco's Modified Eagle's medium (H-DMEM, Hyclone, USA) supplemented with 10% fetal bovine serum (FBS) and 1% penicillin/streptomycin solution. The medium was

Downloaded from https://academic.oup.com/rb/advance-article/doi/10.1093/rb/rbab054/6381593 by Viikki Science Library user on 07 October 2021

refreshed every other day. Cells at passage 12 were applied in this study. Before experiments, samples were sterilized by exposure to ^{60}Co irradiation. Afterward, the extracts of samples were obtained according to the international standard ISO 10993-12:2002. In brief, membranes were added with H-DMEM medium in 1.25 cm^2/mL ratio and then incubated for 24 h. Cells were first seeded at about 30% confluency. The next day cell culture medium was replaced by the extract supplemented with 10% FBS and 1% penicillin/streptomycin solution. Cells cultured in the normal medium served as the control. To evaluate the proliferation of CCC-ESF-1, Calcein-AM (Dojindo, Japan) staining were carried out after cells were treated with extract for 1, 2, and 3 day(s). In brief, cells were washed with PBS, added with the work solution, and kept in the incubator for 15 min. After that, they were observed under an inverted fluorescence microscope (Zeiss, Germany).

Furthermore, Cell Counting Kit-8 (CCK-8, Dojindo, Japan) assay was performed to detect the potential cytotoxicity of the extract on cells. Cells were seeded and treated as described above. After incubation for 1, 2, and 3 day(s), the cell medium was changed with 110 μL normal medium containing 10 μL CCK-8. After 2 h, Optical density (OD) at 450 nm was measured under a microplate reader (BioTek, USA).

2.9 Statistical analysis

IBM SPSS statistics 22 was used to analyze the data statistically. All the experiments were conducted in triplicate. One-way analysis of variance (ANOVA) followed by post hoc comparisons with the least significant difference (LSD) method was adopted, and $p < 0.05$ was considered statistically significant.

Downloaded from https://academic.oup.com/rb/advance-article/doi/10.1093/rb/rbab054/6381593 by Viikki Science Library user on 07 October 2021

3. Results and discussions

3.1 Surface morphology and compositions of BC-TA-Mg composites

The surface morphology of membranes was displayed in Fig. 2a. BC showed a nanofiber network structure, and the orientation of nanofibers was random. As for the composite membranes, TA and $MgCl_2$ particles were found to adhere to the nanofibers. With the increase of Mg^{2+} concentration, the number of attached particles increased. BC-TA-6Mg composites showed the largest number of particles attached to the nanofibers, and some of the nanofibers were even totally covered by the particles.

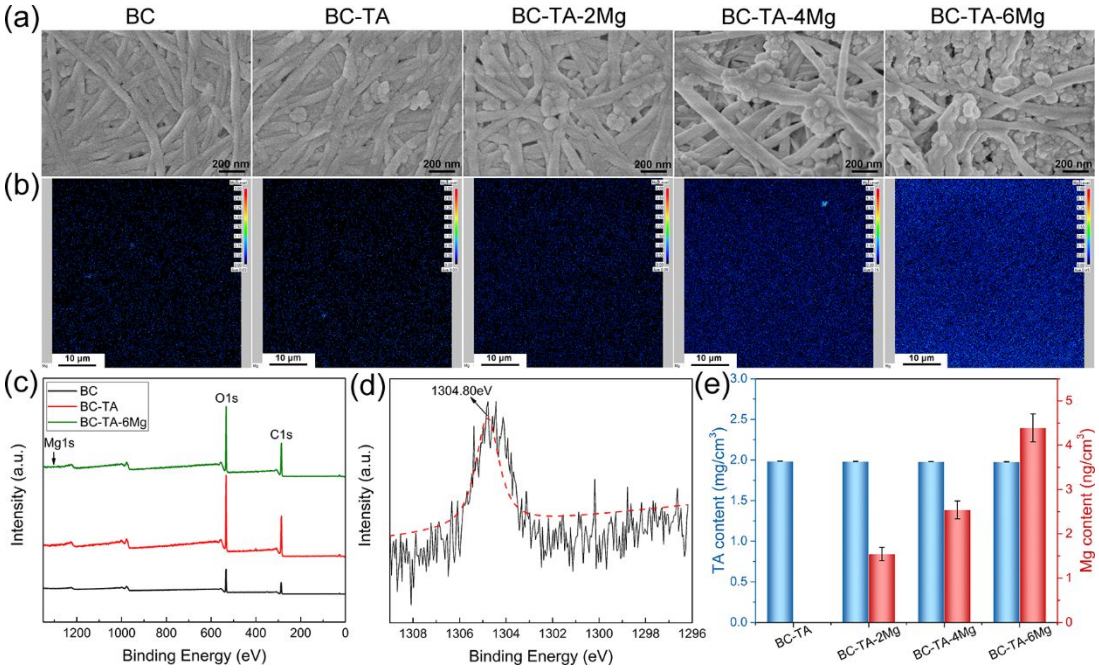

Fig. 2 SEM images (a) and Mg elements distribution detected by EPMA (b) of BC, BC-TA, BC-TA-2Mg, BC-TA-4Mg, and BC-TA-6Mg membranes. (c) XPS survey spectra of BC, BC-TA, and BC-TA-6Mg membranes. (d) High-resolution XPS spectra of Mg 1s. (e) The content of TA and Mg in different samples.

Fig. 2b exhibits the distribution of Mg element on different samples detected by EPMA.

Downloaded from https://academic.oup.com/rb/advance-article/doi/10.1093/rb/rbab054/6381593 by Viikki Science Library user on 07 October 2021

There were no Mg on the BC and BC-TA membranes. Mg elements were found on BC-TA-Mg membranes, and they were distributed homogeneously across the surface. Furthermore, the Mg content varied for different samples. Just as expected, BC-TA-2Mg showed the lowest content of Mg, and BC-TA-6Mg displayed the highest content of Mg. The results verified the successful introduction of TA and Mg^{2+} on BC.

The surface composition of BC, BC-TA, and BC-TA-6Mg samples was determined by XPS. The survey spectra (Fig. 2c) revealed two major peaks at 286.7 and 533.1 eV, assigned to C 1s and O 1s, respectively. This suggested that C and O were the main elements of BC, BC-TA, and BC-TA-Mg membranes. The high-resolution spectra of Mg 1s in BC-TA-6Mg composite were detected, and the fitted curve displayed a peak at 1304.80 eV, indicating the existence of $MgCl_2$ in BC-TA-6Mg composite [29].

The content of TA and Mg in different samples was shown in Fig. 2d. BC-TA and BC-TA-Mg composites showed almost the same amount of TA (1.984 ± 0.001 mg/cm^2 for BC-TA, 1.981 ± 0.003 mg/cm^2 for BC-TA-2Mg, 1.978 ± 0.001 mg/cm^2 for BC-TA-4Mg, and 1.977 ± 0.002 mg/cm^2 for BC-TA-6Mg), while the content of Mg was different for different samples. The content of Mg for BC-TA, BC-TA-2Mg, BC-TA-4Mg, and BC-TA-Mg was 0.00 ± 0.001, 1.54 ± 0.15, 2.54 ± 0.20, and 4.39 ± 0.31 ng/cm^2, respectively. The results were in agreement with those detected by EPMA.

3.2 Surface roughness and surface wettability of BC-TA-Mg composites

AFM was conducted to record the surface roughness of the membranes. Fig. 3a presents the three-dimensional AFM images of five different membranes, and Fig. 3c displays the histogram of Ra. All the samples revealed the nanofiber network structure. The Ra

Downloaded from https://academic.oup.com/rb/advance-article/doi/10.1093/rb/rbab054/6381593 by Viikki Science Library user on 07 October 2021

of BC-TA (24.0 ± 0.3 nm) and BC-TA-2Mg (25.5 ± 3.1 nm) was not significantly different from that of pure BC (21.4 ± 1.8 nm). However, the Ra of BC-TA-4Mg (25.5 ± 1.2 nm) and BC-TA-6Mg (31.0 ± 3.9 nm) significantly increased compared to that of pure BC. More $MgCl_2$ particles were anchoring on the surfaces of BC nanofibers for BC-TA-4Mg and BC-TA-6Mg samples, resulting in increased Ra of the composites.

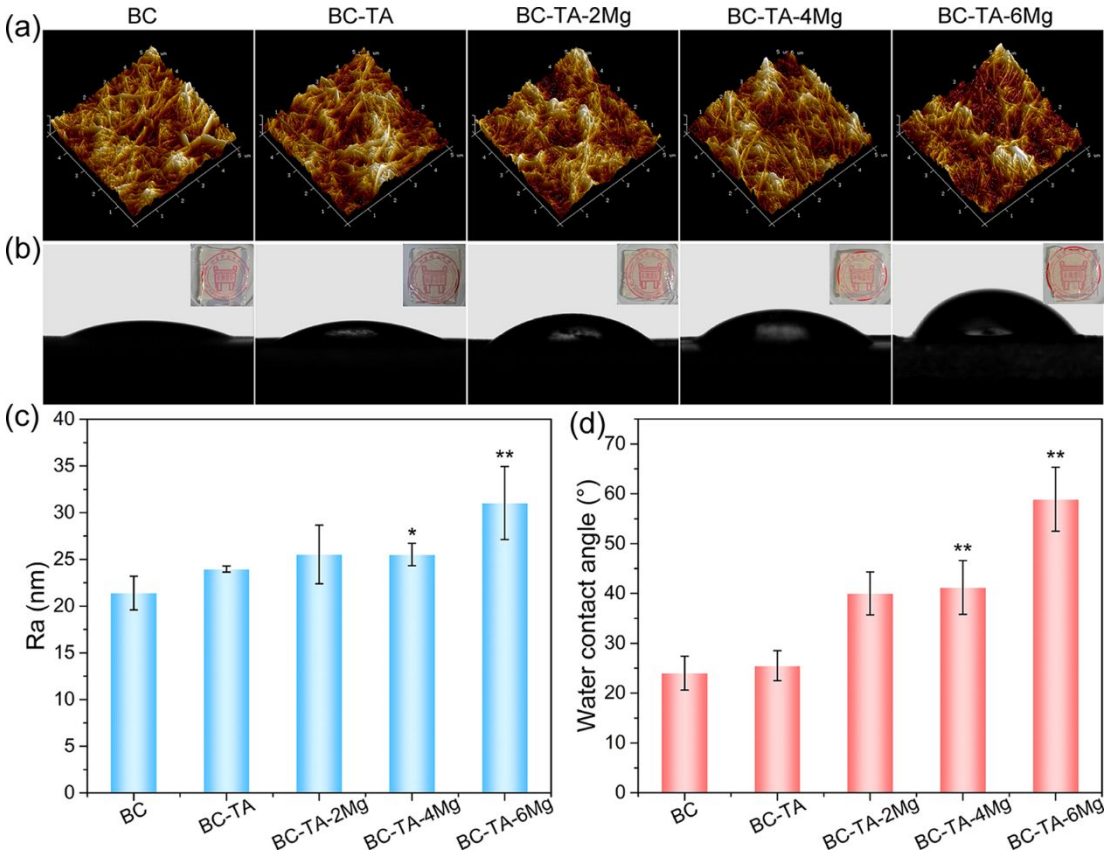

Fig. 3 AFM images (a) and water contact angles images (b) of BC, BC-TA, BC-TA-2Mg, BC-TA-4Mg, and BC-TA-6Mg membranes. The inserted pictures in (b) were the photographs of five membranes. The histogram of Ra (c) and water contact angle (d) of different samples. *$p < 0.05$ compared with BC group, **$p < 0.01$ compared with BC group.

Downloaded from https://academic.oup.com/rb/advance-article/doi/10.1093/rb/rbab054/6381593 by Viikki Science Library user on 07 October 2021

Fig. 3bd exhibits surface wettability of membranes. Pure BC, with a water contact angle of 24.0 ± 3.4°, displayed high hydrophilicity, which may be attributed to large hydroxyl groups (–OH) contained in BC molecules. After the introduction of TA, the water contact angle of the membranes (25.5 ± 3.0°) was not significantly changed. Since TA molecules contain lots of phenolic hydroxyl groups, the BC-TA composite membranes also showed high hydrophilicity. The membranes got less hydrophilic when Mg^{2+} was incorporated into the BC matrix. As the content of Mg^{2+} increased, water contact angle increased from 40.0 ± 4.0° for BC-TA-2Mg to 58.9 ± 6.4° for BC-TA-6Mg. It was considered that some hydrophilic groups contained in BC-TA membranes were covered by the incorporated $MgCl_2$ particles, resulting in decreased hydrophilicity of the composites.

The inserted pictures in Fig. 3b were the photographs of five different membranes. Pure BC was transparent, and the introduction of TA and $MgCl_2$ did not influence the transparency of the membranes. Most BC-based membranes would become opaque after incorporating with antibacterial agents like silver nanoparticles [18] and copper nanoparticles [30], making it inconvenient for wound inspection when used as wound dressings. In comparison, the fabricated BC-TA-Mg in this study were still transparent, which was beneficial for wound inspection.

3.3 FTIR spectrum, thermal stability, mechanical properties, water absorption, water retention capacity, and releasing behavior of BC-TA-Mg composites

FTIR spectrum of all the samples were shown in Fig. 4a.The FTIR spectrum of BC exhibited two characteristic peaks at 3343 and 2893 cm^{-1}, corresponding to stretching

Downloaded from https://academic.oup.com/rb/advance-article/doi/10.1093/rb/rbab054/6381593 by Viikki Science Library user on 07 October 2021

vibration of –OH and $–CH_2–$ group, respectively [27, 30]. In addition, the peaks at 1158 and 1054 cm^{-1} was consistent with skeletal vibration of C–O–C pyranose ring [27, 30]. For TA, a broad adsorption between 3500 and 3000 cm^{-1} were detected, ascribed to the stretching vibration of phenolic group. A peak located at 1712 cm^{-1} was ascribed to C═O stretching, and peaks at 1615, 1536, and 1449 cm^{-1} corresponded to aromatic C–C stretching. Peaks at 1207 and 1034 cm^{-1} were associated with vibration of substituted benzene ring, and those at 1342 and 759 cm^{-1} were attributed to O–H vibration [20, 31, 32]. The spectrum of BC-TA and BC-TA-Mg composites displayed BC's characteristic peaks at 3345, 2893, 1158, and 1054 cm^{-1}. Moreover, typical peaks of TA at 1615, 1207 and 759 cm^{-1} were also detected on BC-TA and BC-TA-Mg composites, indicating successful introduction of TA in BC.

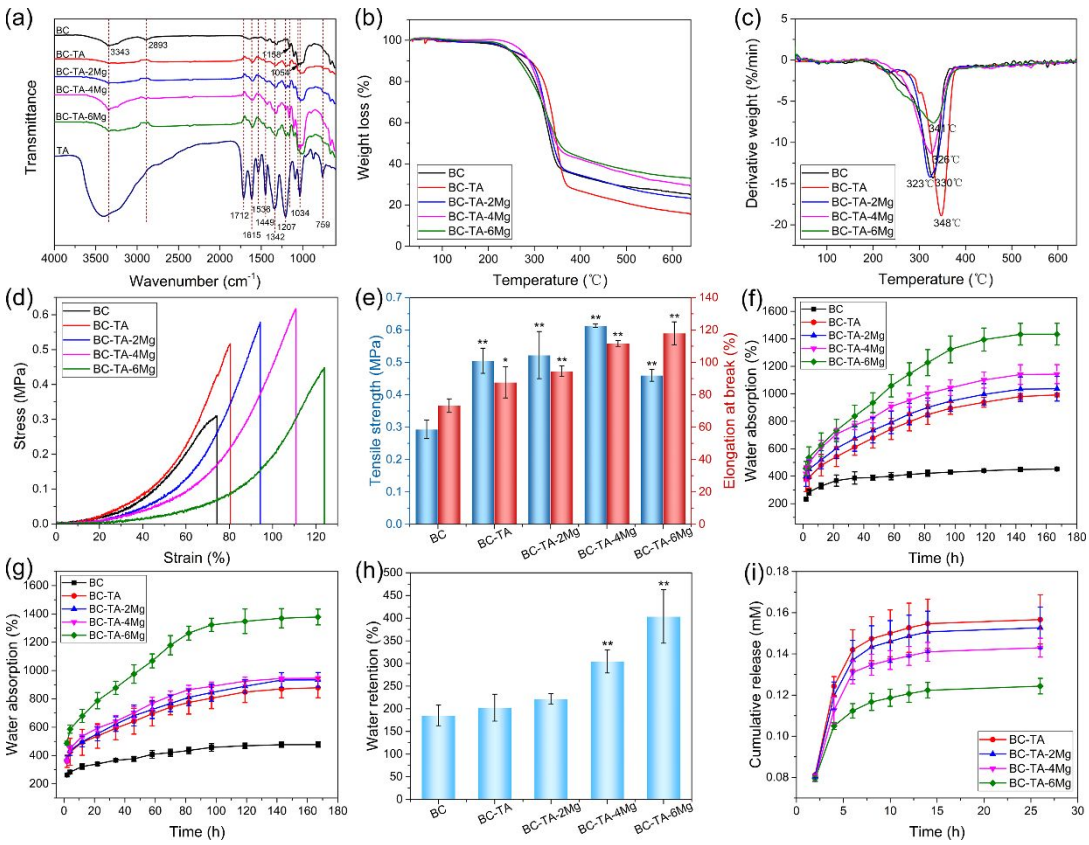

Downloaded from https://academic.oup.com/rb/advance-article/doi/10.1093/rb/rbab054/6381593 by Vilkki Science Library user on 07 October 2021

Fig. 4 (a) FTIR spectrum of BC, BC-TA, BC-TA-2Mg, BC-TA-4Mg, and BC-TA-6Mg membranes. Weight loss (b) and derivative weight (c) of different samples. Tensile stress-strain curves (d) and histogram of tensile strength and elongation at break (e) of different samples. Water absorption capacity of different samples at pH 5 (f) and pH 8 (g). (h) Water retention rate of different samples. (i) *In vitro* release curve of TA from BC-TA and BC-TA-Mg composites. *$p < 0.05$ compared with BC group, **$p < 0.01$ compared with BC group.

The thermal stability of pure BC and composite membranes was detected by thermogravimetric analysis test, and results are presented in Fig. 4bc. The thermal degradation curve of all the five membranes displayed only one significant weight loss stage at 300 ℃ to 400 ℃. During this stage, BC went through depolymerization and decomposition of glucosyl units [33]. It can be observed from the thermal degradation curve that the residue for different samples was different. BC showed a residue of 25.09%. The amount of residue for BC-TA membranes was lower than that of pure BC, namely 15.46%. Concerning samples containing Mg^{2+}, the residue ranged from 22.97% for BC-TA-2Mg to 32.87% for BC-TA-6Mg, indicating that the more Mg^{2+} in the samples increased the membrane residue.

Fig. 4d presents the tensile stress-strain curves of BC, BC-TA, and BC-TA-Mg membranes. A tensile strength of 0.29 ± 0.03 MPa and an elongation at break of 73.26 ± 4.21% were reported for pure BC membranes (Fig. 4e). All the composite membranes displayed significantly higher tensile strength and elongation at break compared to pure

Downloaded from https://academic.oup.com/rb/advance-article/doi/10.1093/rb/rbab054/6381593 by Viikki Science Library user on 07 October 2021

BC membranes. BC-TA-4Mg membranes exhibited the highest tensile strength (0.61 ± 0.01 MPa), and BC-TA-6Mg membranes demonstrated the highest elongation at break (117.98 ± 7.07%) (Fig. 4e). The improved mechanical properties may be attributed to the TA and $MgCl_2$ particles attached to BC nanofibers. As shown in Fig. 2a, TA and $MgCl_2$ particles closely adhered to BC nanofibers, which contributed to the improved mechanical properties of the membranes. Similar phenomena have been found in BC/poly(dopamine) composite membranes [34]. The enhancement of mechanical properties promoted the flexibility and malleability of the membranes, which were beneficial for its application in biomedical fields.

Water absorption of the materials at pH 5 and pH 8, mimicking the pH of the healthy and wound skin, respectively, were tested, and the results are shown in Fig. 4fg. At pH 5 and pH 8, all dry membranes exhibited a sharply increased water absorption ratio within the first 22 hours. After that, the water absorption ratio increased gently with time. BC displayed much lower water absorption ratio compared to BC-TA and BC-TA-Mg composites. The final water absorption capacity for pure BC was quite low (452.12 ± 5.35 and 477.25 ± 18.81% at pH 5 and pH 8, respectively). As shown in Fig. 2a, the dried BC membranes displayed collapsed structure. A large number of H-bonds were contained in BC, and H-bonds tightly connected nanofibers of BC. Therefore, the dried membranes displayed smaller inner space [35], which was adverse for water molecules to enter into. Moreover, strong H-bonds stopped water molecules from breaking them. Thus less water entered into the membranes [28]. The introduction of TA and Mg^{2+} significantly improved the water absorption ratio of the membranes, and

Downloaded from https://academic.oup.com/rb/advance-article/doi/10.1093/rb/rbab054/6381593 by Viikki Science Library user on 07 October 2021

the more Mg^{2+} contained in the membranes, the higher water absorption ratio the membranes displayed. At pH 5, the water ratio was 991.33 ± 13.49%, 1036.79 ± 89.70%, 1142.76 ± 69.38%, and 1434.05 ± 79.42% for BC-TA, BC-TA-2Mg, BC-TA-4Mg, and BC-TA-6Mg, respectively. At pH 8, the value for BC-TA, BC-TA-2Mg, BC-TA-4Mg, and BC-TA-6Mg was 878.52 ± 70.73%, 934.16 ± 51.84%, 945.93 ± 10.58%, and 1377.74 ± 55.64%, respectively. The incorporated TA and $MgCl_2$ particles were covered on the surfaces of the nanofibers, thus reducing the H-bonds between them [28], making it easier for water to enter into the matrix. The above data revealed that BC-TA-Mg composites exhibited strong water absorption capacity in a healthy and wound skin environment.

Fig. 4h presents the water retention rate of the samples. BC-TA-4Mg (304.34 ± 25.34%) and BC-TA-6Mg (403.59 ± 58.98%) displayed higher water retention rate compared with pure BC (185.38 ± 22.58%). Ideal wound dressings with high water absorption and retention capacity are beneficial for the absorption of wound exudates. BC-TA-Mg composites displayed higher water absorption and retention capacity than BC, making it better for them to absorb wound exudates when used as wound dressings.

Fig. 4i displays the release curve of TA from BC-TA and BC-TA-Mg composites. All membranes revealed a rapid release of TA during the first 2 h. The release of TA decreased gradually as time went on. Moreover, as Mg^{2+} concentration in the materials increased, the release of TA decreased. The results were consistent with our previous results [20], suggesting that the controlled release of TA depended on Mg^{2+} concentration. The incorporation of Mg^{2+} in BC-TA membranes conduced to the

Downloaded from https://academic.oup.com/rb/advance-article/doi/10.1093/rb/rbab054/6381593 by Viikki Science Library user on 07 October 2021

chelation of BC, TA, and Mg^{2+}, interfering with TA release [20]. Similar results have been shown by a previous study, verifying that the release of TA from carboxylated agarose composite hydrogels was decreased by ionic interaction [31]. Hydrogels containing Zn^{2+} cross-links displayed more TA release, while materials without Zn^{2+} revealed less TA release.

3.4 Establishment of a multispecies biofilm model *in vitro*

Few studies have investigated the interspecific relationship between *S. aureus* and *P. aeruginosa*, primarily due to the difficulty of getting the two strains to grow together under experimental conditions. Previous studies had shown that when *P. aeruginosa* was cultured with *S. aureus* in LB broth, trypsin soy broth, brain heart extract, or other media, it quickly killed *S. aureus* [36, 37]. Although *S. aureus* and *P. aeruginosa* could not grow together under the experimental plankton-like environments, they are usually simultaneously found in wound infections [38]. The co-presence of *S. aureus* and *P. aeruginosa* lead to disordered and delayed wound healing, thus bringing a heavier burden to patients [39].

The establishment method of multispecies biofilm model *in vitro* is shown in Fig. 5b, and bacteria species incubated in ordinary tryptic soy broth medium (Fig. 5a) was used as control. For the control group, after incubation for 48 h, *S. aureus* suspension became turbid, and the primary biomass was deposited at the bottom of the test tube (Fig. 5c). As for *P. aeruginosa*, a pale green biofilm formed at the gas-liquid junction, and the liquid in the test tube also became cloudy (Fig. 5c). The co-culture of *S. aureus* and *P. aeruginosa* for 48 h resulted in the combination of the above two: the primary biomass

Downloaded from https://academic.oup.com/rb/advance-article/doi/10.1093/rb/rbab054/6381593 by Viikki Science Library user on 07 October 2021

of *S. aureus* deposited at the bottom of the test tube and a pale green biofilm of *P. aeruginosa* formed at the gas-liquid junction (Fig. 5c).

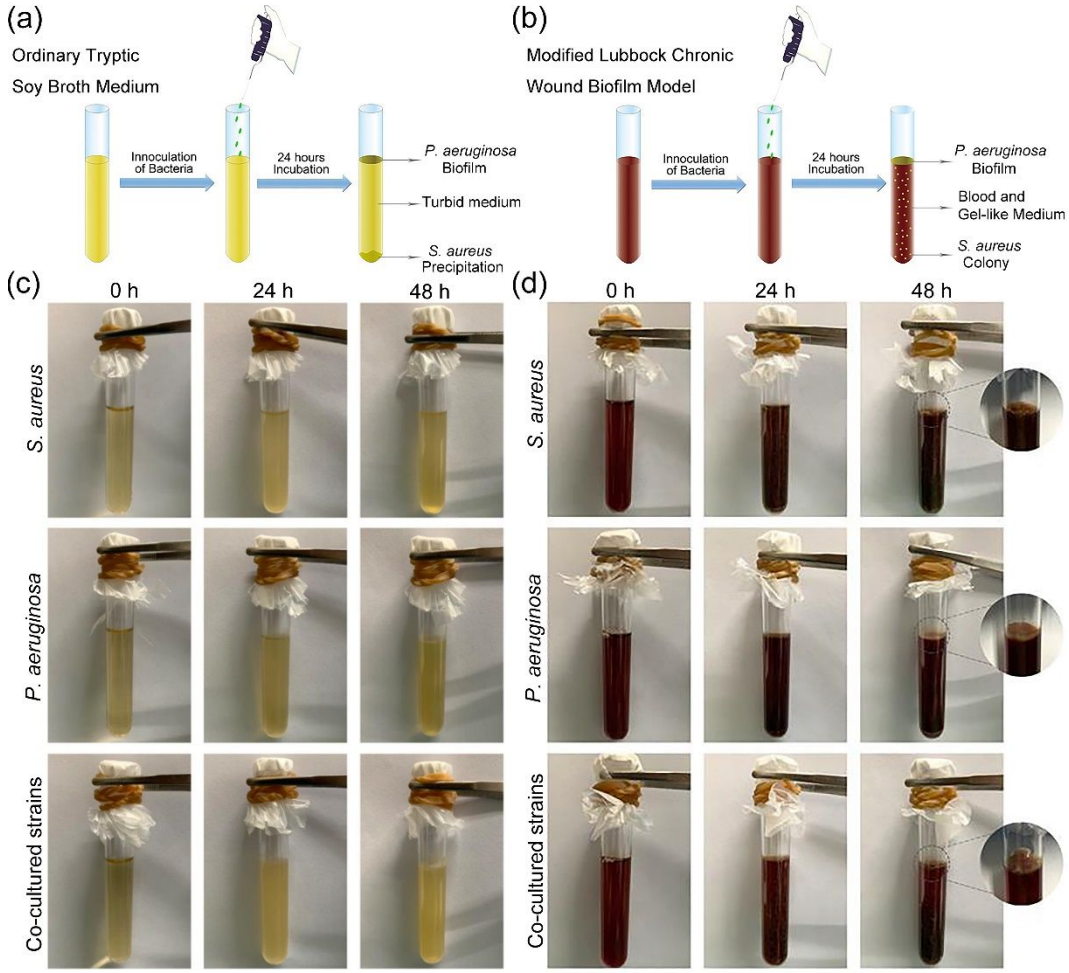

Fig. 5 Schematic illustration for the establishment method of multispecies biofilm model *in vitro*: bacteria were incubated in ordinary tryptic soy broth medium (a) and modified medium (b). The formation of chronic wound biofilms *in vitro*: bacteria were incubated in ordinary tryptic soy broth medium (c) and modified medium (d).

The modified medium consisted of lysed red blood cells, plasma, and a medium made from minced meat (TSB medium), which was used to simulate the nutrients in the wound environment. After incubation for 48 h in the modified medium, *S. aureus*

Downloaded from https://academic.oup.com/rb/advance-article/doi/10.1093/rb/rbab054/6381593 by Viikki Science Library user on 07 October 2021

formed a jelly-like substance, and the bacterial colonies evenly dispersed in the jelly-like gelatin (Fig. 5d). Unlike the control group, there was no biomass deposition at the bottom of the test tube. After 48 h' culture, *P. aeruginosa* formed a pale green biofilm at the gas-liquid junction, and the liquid in the test tube remained liquid without condensation (Fig. 5d). As for the co-cultured *S. aureus* and *P. aeruginosa*, bacterial colonies of *S. aureus* evenly dispersed in the gel, and a pale green biofilm formed at the gas-liquid junction (Fig. 5d).

The results showed that if the inoculant contained a coagulase-positive bacterial species (e.g., *S. aureus*), the liquid medium would coagulate into a jelly-like substance after incubation for about 16 hours (Fig. 5d). This is because *S. aureus* could activate the coagulation cascade through secreting staphylococcus coagulase. Staphylococcus coagulase binds to prothrombin, forming a complex named *Staphylococcus* thrombin. Thereafter, the complex converts soluble fibrinogen into insoluble fibrin chain [40]. *P. aeruginosa* could grow in this medium, but the medium does not coagulate because *P. aeruginosa* lacks the ability to secret coagulase, thus unable to activate the coagulation cascade. Therefore, in this study, coagulated plasma can be used as a carrier for bacterial adhesion and residence, which was considered to be more close to the actual wound environment of the human body.

In this *in vitro* model of multispecies biofilm, the bacterial biofilm of co-cultured *S. aureus* and *P. aeruginosa* grew, developed, and matured rapidly. Furthermore, this method is easy to operate and is with low cost, thus displaying certain advantages in the field of developing chronic wound biofilm models.

Downloaded from https://academic.oup.com/rb/advance-article/doi/10.1093/rb/rbab054/6381593 by Viikki Science Library user on 07 October 2021

3.5 Establishment of a biofilm on an artificial wound bed

As far as we know, quite a few studies reported applying *in vitro* model to test any materials' anti-biofilm function. An anti-biofilm model is urgently needed to evaluate the efficiency of solid antibacterial materials. In this study, the *in vitro* multispecies biofilm model established by the above methods was adopted. The pre-cultured biofilm was transferred to an artificial wound bed, and the applicability of wound dressings on the model was tested as shown in Fig. 6a. Fig. 6b shows that chronic wounds biofilm of *S. aureus*, *P. aeruginosa*, and co-cultured *S. aureus* and *P. aeruginosa* efficiently proliferated and matured on the artificial wound bed. This efficient proliferation and maturation demonstrated that the *in vitro* artificial wound bed model with a biofilm on its surface can be used to evaluate the anti-biofilm activities of wound dressings. This model is crucial for the early-stage research and development of wound dressings. Moreover, it was simple and economical to evaluate the anti-biofilm activities of any material except wound dressings.

Downloaded from https://academic.oup.com/rb/advance-article/doi/10.1093/rb/rbab054/6381593 by Viikki Science Library user on 07 October 2021

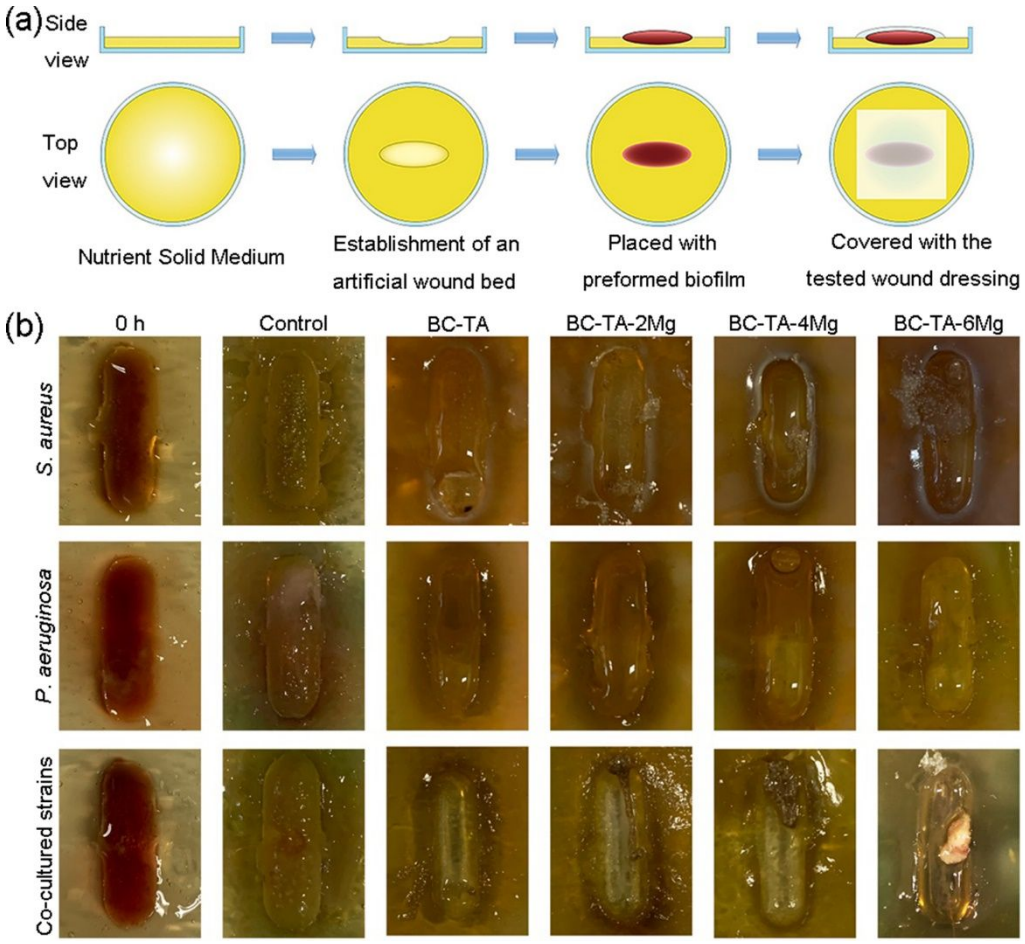

Fig. 6 (a) Schematic illustration for the establishment of biofilm on the artificial wound bed. (b) Photographs of biofilms on artificial wound bed before and after treatment with BC-TA-Mg composites for 24 h.

3.6 SEM observation of biofilm

The biofilm of singly-cultured *S. aureus*, *P. aeruginosa*, and co-cultured *S. aureus* and *P. aeruginosa* was observed by SEM after incubated on an artificial wound bed for 24 h. Fig. 7 shows that for all the three groups, the bacterial cells were embedded with some EPS. The co-cultured strains displayed both rod-shaped *P. aeruginosa* and spherical S. *aureus* in the matrix. Besides, the biofilm was constituted of cross-linked

Downloaded from https://academic.oup.com/rb/advance-article/doi/10.1093/rb/rbab054/6381593 by Viikki Science Library user on 07 October 2021

bacterial cells and the EPS. The results were similar to a previous report [25].

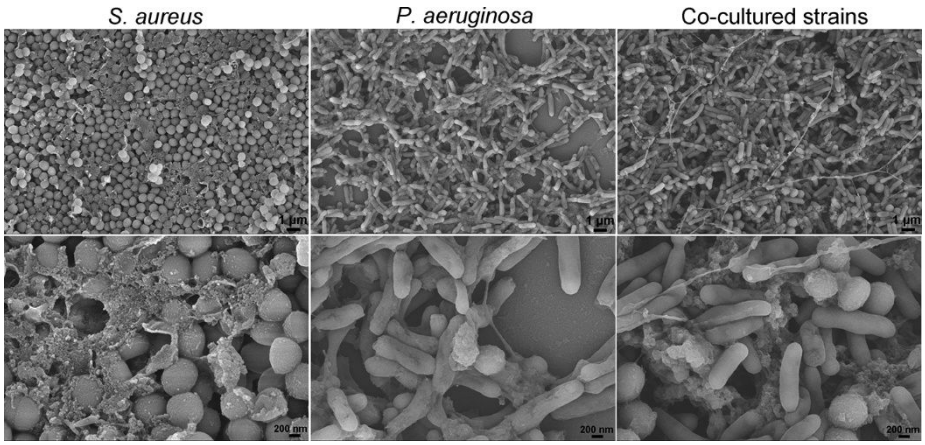

Fig. 7 SEM images of the biofilm model of singly-cultured *S. aureus*, *P. aeruginosa*, and co-cultured *S. aureus* and *P. aeruginosa*. The images were taken at two different magnifications of 5000 × and 20000 × .

3.7 Effects of BC-TA-Mg composites on biofilms *in vitro*

Fig. 6b shows that singly-cultured *S. aureus* on the artificial wound bed in the control group quickly proliferated and matured, and there were many biofilms in the middle and edge of the wound bed. The amount of biofilm formation was significantly reduced in all the experimental groups. The biomass reduction was the most significant in the BC-TA composite-treated group. In the BC-TA-2Mg and BC-TA-4Mg composite-treated group, a small number of biofilms existed in the middle and edge of the artificial wound bed. There were still some bacterial biofilms in the middle and edge of the wound bed for the BC-TA-6Mg group. The results indicate that BC-TA composite material showed the best inhibitory effect on *S. aureus* biofilms, followed by BC-TA-2Mg, BC-TA-4Mg, and BC-6Mg in sequence.

Downloaded from https://academic.oup.com/rb/advance-article/doi/10.1093/rb/rbab054/6381593 by Viikki Science Library user on 07 October 2021

Singly-cultured *P. aeruginosa* on the artificial wound bed in the control group also proliferated rapidly and matured. Many of the produced biofilms presented in the middle and the edge of the wound bed, and some areas at the edge of the wound bed became significantly green, indicating a lot of pyocyanin production in the biofilms. BC-TA, BC-TA-2Mg, BC-TA-4Mg, and BC-TA-6Mg significantly inhibited biofilm production and BC-TA exhibited the best inhibitory effect.

The results were similar for the co-cultured *S. aureus* and *P. aeruginosa* with efficient proliferation and maturation in the wound bed. The edge area of the wound bed appeared to be green, suggesting the production of pyocyanin. The number of biofilms for the group treated with BC-TA was significantly reduced, followed by BC-TA-2Mg and BC-TA-4Mg treated group. For the BC-TA-6Mg treated group, there was still a tiny piece of slimy bacterial biofilms existing in the middle of the wound bed, indicating that the inhibitory effect of BC-TA-6Mg on biofilm was inferior to that of BC-TA-2Mg and BC-TA-4Mg.

3.7.1 Gram staining

In this study, gram staining was used to evaluate the inhibitory effect of BC-TA-Mg composite materials on bacterial biofilm formation. After gram staining, gram-positive *S. aureus* biofilms appeared purple, while gram-negative *P. aeruginosa* biofilms showed a red color. Fig. 8a shows a large number of *S. aureus* or *P. aeruginosa* biofilms formed in the control group. The amount of biofilm was significantly reduced after treatment with the composite materials. A few sporadic biofilms appeared in the experimental groups, indicating that BC-TA-Mg composites displayed a good

Downloaded from https://academic.oup.com/rb/advance-article/doi/10.1093/rb/rbab054/6381593 by Viikki Science Library user on 07 October 2021

inhibitory effect on *S. aureus* or *P. aeruginosa* biofilm formation. The reduction rate of BC-TA, BC-TA-2Mg, BC-TA-4Mg and BC-TA-6Mg against *S. aureus* biofilm was quantified to 95.56% ± 0.71%, 94.40% ± 1.67%, 93.92% ± 1.53%, and 93.55% ± 1.85%, respectively (Fig. 8b). Besides, for *P. aeruginosa* biofilm, BC-TA, BC-TA-2Mg, BC-TA-4Mg, and BC-TA-6Mg showed a reduction rate of 91.96% ± 3.78%, 86.35% ± 6.98%, 74.12% ± 8.33%, and 71.36% ± 7.84%, respectively (Fig. 8b).

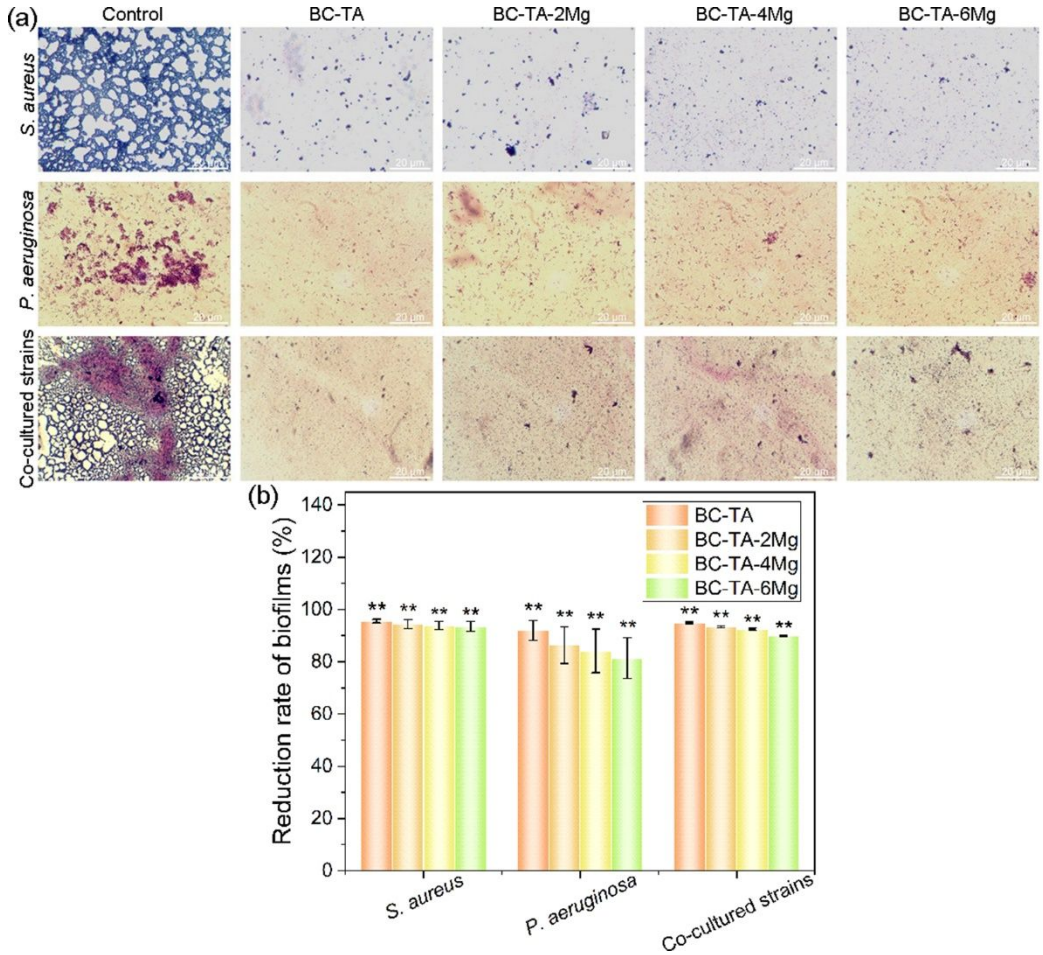

Fig. 8 (a) Gram staining for bacterial biofilm treated with different membranes for 24 h. (b) The quantified reduction rate of stained area based on image data using the software Image-Pro Plus Vision 6.0. $^{**}p < 0.01$ compared with the control group.

Downloaded from https://academic.oup.com/rb/advance-article/doi/10.1093/rb/rbab054/6381593 by Viikki Science Library user on 07 October 2021

When *S. aureus* and *P. aeruginosa* were co-cultured on the wound bed, a large number of *P. aeruginosa* biofilms were stained red and surrounded by purple *S. aureus* biofilms in the control group. This colored orientation confirmed that *S. aureus* and *P. aeruginosa* could be co-cultured in this modified medium, and they could proliferate and mature rapidly. After being treated with composite materials, biofilm formation was significantly reduced, and only small areas were stained purple, indicating that the number of *S. aureus* biofilms was higher than that of *P. aeruginosa* biofilms. In addition, the quantified results (Fig. 8b) shows that BC-TA, BC-TA-2Mg, BC-TA-4Mg, and BC-TA-6Mg exhibited an inhibition rate of 94.94% ± 0.32%, 93.42% ± 0.33%, 92.51% ±0.38 %, and 89.89% ± 0.25% against co-cultured biofilms, respectively.

3.7.2 FITC-ConA staining

Fig. 9a shows that for the singly-cultured *S. aureus* and *P. aeruginosa*, there were lots of exopolysaccharides secreted by bacteria in the control group. Treatment with composite materials significantly reduced the number of exopolysaccharides. In the BC-TA group, the amount of green fluorescence was the least. The stained area was also the smallest, suggesting that BC-TA composite material demonstrated the best inhibitory effect on the secretion of exopolysaccharides. When *S. aureus* and *P. aeruginosa* were co-cultured, the number of exopolysaccharides was significantly decreased in all the groups, demonstrating that co-culture of the two bacteria influenced the production of exopolysaccharides.

Downloaded from https://academic.oup.com/rb/advance-article/doi/10.1093/rb/rbab054/6381593 by Viikki Science Library user on 07 October 2021

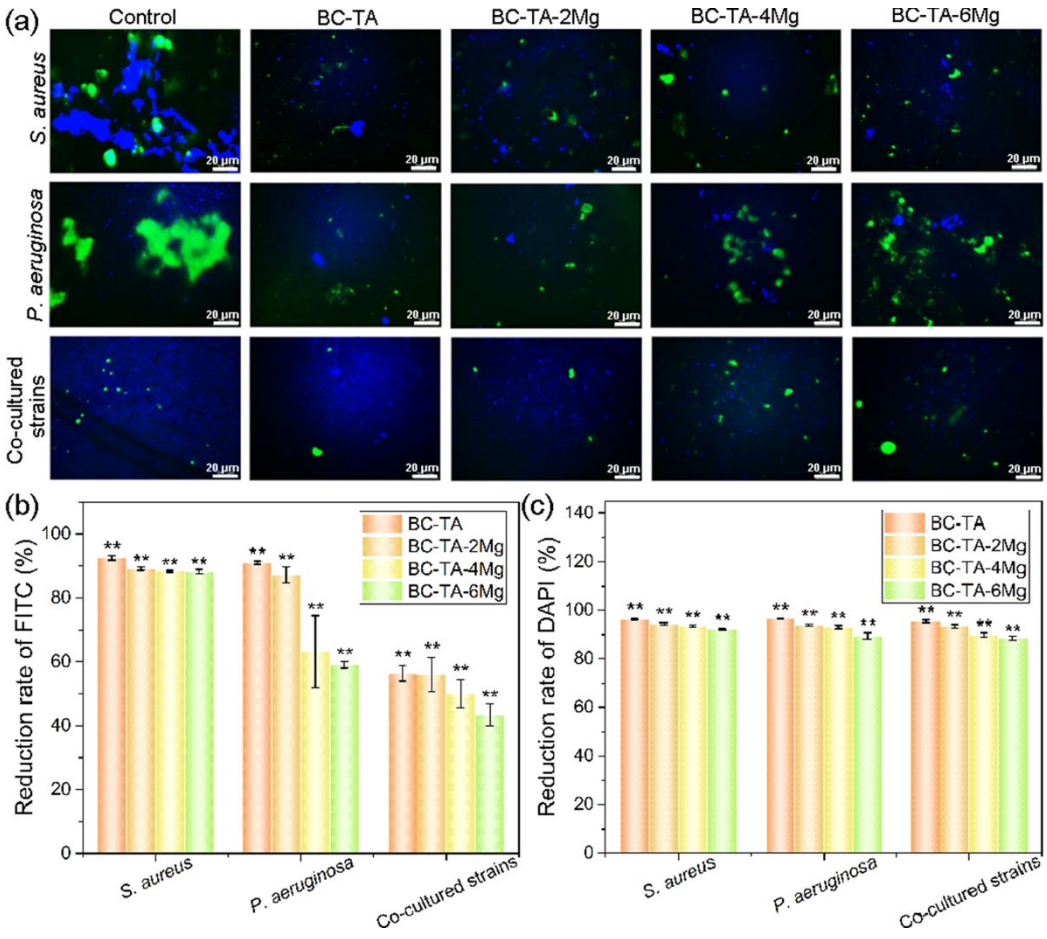

Fig. 9 (a) FITC-ConA and DAPI staining for exopolysaccharides and cell nucleus of bacteria treated with different membranes for 24 h. The quantified reduction rate of intergraded optical density of FITC (b) and DAPI (c) based on image data using the software Image-Pro Plus Vision 6.0. $^{**}p < 0.01$ compared with control group.

The integral optical density of stained polysaccharide and nucleus were quantified, and the reduction rate of integrated optical density compared with the control was calculated as displayed in Fig. 9bc. For singly-cultured *S. aureus*, the number of exopolysaccharides and cell nucleus was significantly decreased when the biofilms were treated with composite materials. Compared to control, the reduction rate of

Downloaded from https://academic.oup.com/rb/advance-article/doi/10.1093/rb/rbab054/6381593 by Viikki Science Library user on 07 October 2021

polysaccharide for BC-TA, BC-TA-2Mg, BC-TA-4Mg, and BC-TA-6Mg was 92.44% ± 0.68%, 89.18% ± 0.48%, 88.37% ± 0.32%, and 88.27% ± 0.70%, respectively. The amount of cell nucleus decreased to 96.20% ± 0.17%, 94.54% ± 0.29%, 93.57% ± 0.38%, and 92.31% ± 0.23% for BC-TA, BC-TA-2Mg, BC-TA-4Mg, and BC-TA-6Mg, respectively. *P. aeruginosa* showed a similar reduction in the amount of polysaccharide and cell nucleus after treatment with composite materials. BC-TA, BC-TA-2Mg, BC-TA-4Mg, and BC-TA-6Mg displayed a polysaccharide reduction rate of 91.02% ± 0.44%, 87.25% ± 2.52%, 63.25% ± 11.26%, and 59.08% ± 1.00%, respectively. The reduction rate of cell nuclei for BC-TA, BC-TA-2Mg, BC-TA-4Mg, and BC-TA-6Mg was 94.40% ± 0.20%, 94.07% ± 0.46%, 93.23% ± 0.68%, and 89.57% ± 1.37%, respectively. As for co-cultured *S. aureus* and *P. aeruginosa*, the amount of polysaccharide and cell nucleus also decreased when bacteria were treated with composite materials. The amount of polysaccharides of BC-TA, BC-TA-2Mg, BC-TA-4Mg, and BC-TA-6Mg treated groups decreased to 56.38% ± 2.37%, 56.08% ± 5.35%, 49.98% ± 4.43%, and 43.34% ± 3.41% of control, respectively. The number of cell nucleus for BC-TA, BC-TA-2Mg, BC-TA-4Mg, and BC-TA-6Mg was 95.47% ± 0.57%, 93.61% ± 0.66%, 89.97% ± 0.98%, and 88.60% ± 0.71%, respectively.

From the above data, it was concluded that BC-TA-Mg composite materials had an excellent inhibitory effect on the secretion of EPS and proliferation of singly-cultured *S. aureus*, *P. aeruginosa*, and co-cultured *S. aureus* and *P. aeruginosa*. Besides, BC-TA displayed the best inhibitory activities.

3.7.3 Plate counting method

Downloaded from https://academic.oup.com/rb/advance-article/doi/10.1093/rb/rbab054/6381593 by Viikki Science Library user on 07 October 2021

Plate counting method was used to evaluate the inhibition rate of BC-TA-Mg composite materials on the bacterial number in the *in vitro* chronic wound biofilm. The number of bacterial colonies on the agar plate can directly reflect the inhibition rate of various samples on the *in vitro* chronic wound biofilms. For singly-cultured *S. aureus*, in the control group, there were a large number of colonies ($7.51\times10^9 \pm 2.88\times10^8$ CFU/mL), and colonies are densely distributed on the agar plate (Fig. 10ab). The number of colonies was largely decreased after treatment with composite materials, namely $2.87\times10^7 \pm 1.73\times10^6$, $3.16\times10^7 \pm 1.24\times10^6$, $5.23\times10^7 \pm 2.38\times10^6$, and $6.78\times10^7 \pm 3.93\times10^6$ CFU/mL for BC-TA, BC-TA-2Mg, BC-TA-4Mg, and BC-TA-6Mg, respectively (Fig. 10b). The calculated antibacterial rate for BC-TA, BC-TA-2Mg, BC-TA-4Mg, and BC-TA-6Mg was 99.62% ± 0.03%, 99.58% ± 0.02%, 99.30% ± 0.04%, and 99.10% ± 0.06%, respectively (Fig. 10b). The data further confirmed that BC-TA-Mg composites exhibited excellent antibacterial activities against *S. aureus*, among which BC-TA had the best inhibitory effect on *S. aureus* biofilm formation. The materials also demonstrated strong anti-biofilm activities against singly-cultured *P. aeruginosa*. The number of colonies for control, BC-TA, BC-TA-2Mg, BC-TA-4Mg, and BC-TA-6Mg was $3.24\times10^8 \pm 3.27\times10^7$, $1.90\times10^6 \pm 5.57\times10^5$ $2.57\times10^6 \pm 5.69\times10^5$, $7.20\times10^6 \pm 8.19\times10^5$ and $1.09\times10^7 \pm 1.81\times10^6$ CFU/mL, respectively (Fig. 10b). Besides, BC-TA, BC-TA-2Mg, BC-TA-4Mg and BC-TA-6Mg showed an antibacterial rate of 99.41% ± 0.17%, 99.21% ± 0.18%, 97.78% ± 0.25%, and 96.63% ± 0.56%, respectively (Fig. 10c). For the co-cultured *S. aureus* and *P. aeruginosa*, the inhibition percentage of BC-TA, BC-TA-2Mg, BC-TA-4Mg, and BC-TA-6Mg composites

Downloaded from https://academic.oup.com/rb/advance-article/doi/10.1093/rb/rbab054/6381593 by Viikki Science Library user on 07 October 2021

against *S. aureus* biofilm was 82.13% ± 1.17%, 74.58% ± 1.39%, 68.90% ± 2.34%, and 61.99% ± 1.60%, respectively (Fig. 10c). The inhibition rate of BC-TA, BC-TA-2Mg, BC-TA-4Mg, and BC-TA-6Mg composites against *P. aeruginosa* was 99.10% ± 0.13%, 97.85% ± 0.22%, 96.41% ± 0.61%, and 94.94% ± 0.38%, respectively (Fig. 10c).

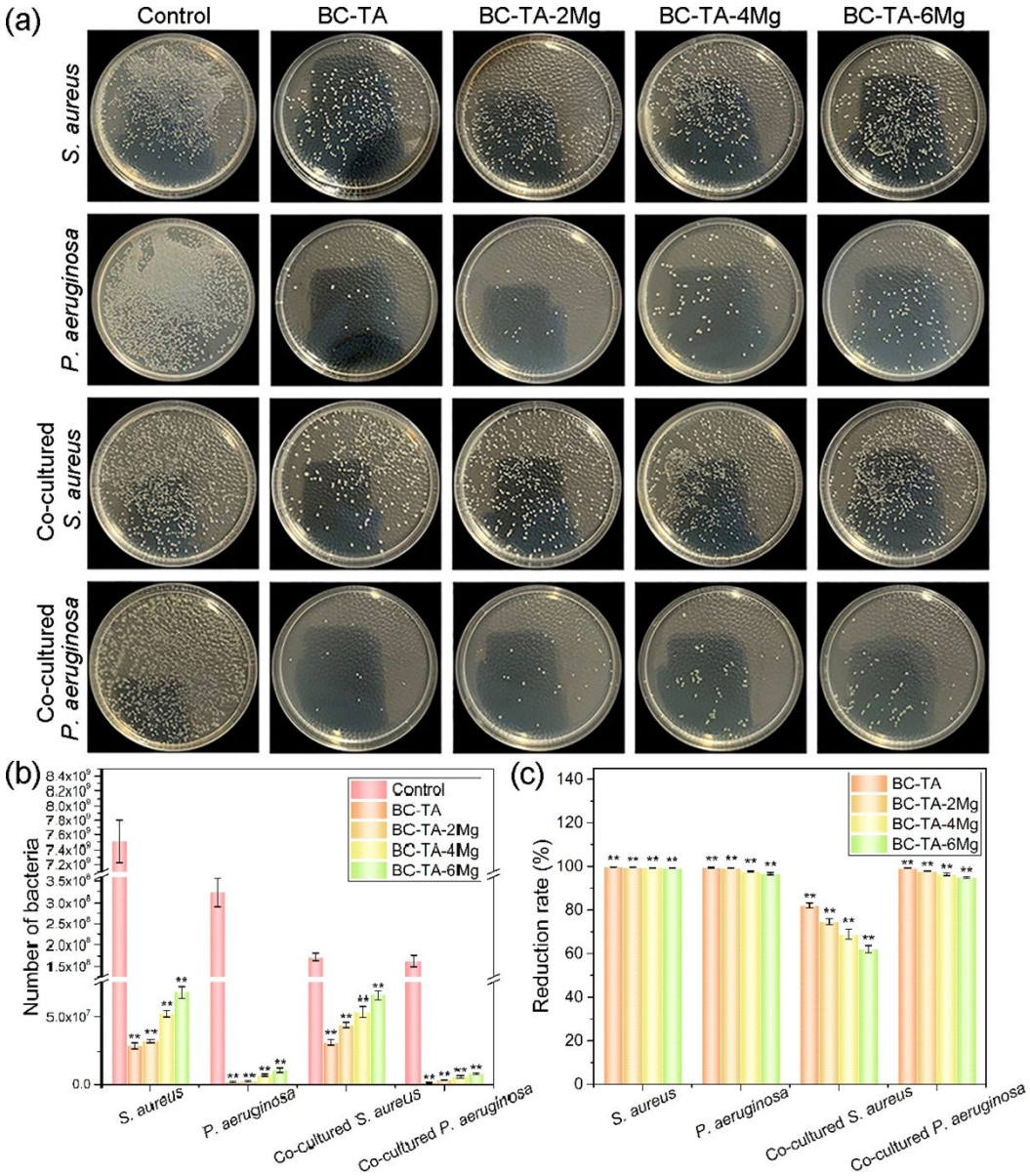

Fig. 10 (a) Photographs of recultivated *S. aureus* and *P. aeruginosa* on agar from singly-cultured biofilm or co-cultured biofilm treated with different membranes for 24 h. Number (b) and reduction rate (c) of bacteria from singly-cultured biofilm or co-

Downloaded from https://academic.oup.com/rb/advance-article/doi/10.1093/rb/rbab054/6381593 by Viikki Science Library user on 07 October 2021

cultured biofilms treated with different membranes for 24 h. $^{**}p < 0.01$ compared with control group.

The plate counting method results demonstrated that BC-TA-Mg composite materials exhibited potent inhibitory activities on biofilm of singly-cultured *S. aureus*, *P. aeruginosa*, and co-cultured *S. aureus* and *P. aeruginosa*. Moreover, BC-TA composite material remained the best inhibitory material, followed by BC-TA-2Mg, BC-TA-4Mg, and BC-6Mg in sequence.

Considering the interactions between BC composites and the *in vitro* biofilm model, the membranes were further observed by SEM after treating the biofilm. Supplementary Fig. S1 showed that for singly-cultured *S. aureus*, *P. aeruginosa*, and co-cultured *S. aureus* and *P. aeruginosa*, no bacteria or biofilm adhered or penetrated on BC-TA and BC-TA-Mg composites. Therefore, based on the results of Gram staining, FITC-ConA staining and plate counting method, it was concluded that BC-TA composite showed the best inhibitory effect on the formation of biofilms of singly-cultured *S. aureus*, *P. aeruginosa*, and co-cultured *S. aureus* and *P. aeruginosa*. The introduction of Mg^{2+} decreased the anti-biofilm activities of the composite since it showed a more controlled TA release [20]. The results were consistent with our previous study [20]. As for singly-cultured *P. aeruginosa* and the co-cultured system, *P. aeruginosa* secreted a number of phenazine compounds, including green pyocyanin [41]. Fig. 5c displays that the biofilm of singly-cultured *P. aeruginosa* and co-cultured system was pale green, suggesting the presence of pyocyanin. Pyocyanin plays essential roles in a number of significant

Downloaded from https://academic.oup.com/rb/advance-article/doi/10.1093/rb/rbab054/6381593 by Viikki Science Library user on 07 October 2021

biological activities in *P. aeruginosa*. It influences gene expression, and it maintains fitness of bacterial cells [42]. It is also involved in bacterial respiration. The biofilm formation of *P. aeruginosa* is also maintained by pyocyanin [42]. It increased the resistance of *P. aeruginosa* to antimicrobial agents [42]. This study found that the inhibition of BC-TA-Mg composites on singly-cultured *S. aureus* biofilm was better than that on biofilm of singly-cultured *P. aeruginosa* and co-cultured system (Fig. 8 and Fig. 9ab). The reason may be that the secreted pyocyanin by *P. aeruginosa* increased its resistance to BC-TA-Mg composites. TA has broad-spectrum antibacterial properties, inhibiting the proliferation of microorganisms like *S. aureus*, *P. aeruginosa*, and *Escherichia coli* [43]. TA inhibits the proliferation of bacteria by destroying the cell wall and cytoplasm of bacteria, and it also inhibits protease activities by inducing complexation with enzymes or substrates [44]. On the other hand, TA is able to chelate with metal ions, therefore it could chelate with iron ions contained in the culture medium. Microorganisms that grow under aerobic conditions need iron for conducting some essential functions, such as reducing DNA's ribonucleotide precursor and producing heme. Therefore, the inhibitory effect of TA on bacterial growth may also be attributed to its strong ability to chelate with iron ions [45].

It has been reported that TA inhibited the formation of *S. aureus* biofilm, and the inhibition rate was up to 60% at 2 μM [46]. TA also shows good inhibition on *P. aeruginosa* biofilm [47, 48], and the inhibition efficiency depended on bacterial density and nutrient conditions [48]. Previous studies reported several possible mechanisms about the inhibitory effects of TA on bacterial biofilms. Chusri *et al.* [49] clarified that

Downloaded from https://academic.oup.com/rb/advance-article/doi/10.1093/rb/rbab054/6381593 by Viikki Science Library user on 07 October 2021

TA inhibited the formation of *S. aureus* biofilm by altering the structure of cell walls and cell surface hydrophobicity of the bacteria. Lee *et al.* [22] proved that anti-biofilm activities of TA might be attributed to suppressed expressions of a quorum-sensing gene (*agrA*), two intercellular adhesion genes (icaA and icaD) and two virulence-regulatory genes (*sigB* and *sarA*) in *S. aureus*. Payne *et al.* [46] proved that TA promoted extracellular transglycosylase IsaA levels, thus inhibiting the formation of *S. aureus* biofilm in multiple biofilm models. TA is a powerful quorum sensing (QS) inhibitor, which is an anti-biofilm mechanism of TA [50, 51]. QS system is an essential channel for information communication between bacteria. Many bacterial functions such as virulence factors secretion, secondary metabolites production, and biofilms maturation are regulated by this system [52]. QS inhibitors can effectively inhibit bacterial adhesion and dispersal [52]. TA inhibited QS in *P. aeruginosa* by suppressing *N*-acylhomoserine lactone synthase production, thus inhibiting biofilm formation [52]. An inhibition in EPS of *P. aeruginosa* by TA has also been proved to contribute to TA's anti-biofilm activities [51]. Further investigations should be done to disclose the possible mechanism under TA's anti-biofilm activities.

3.8 I*n vitro* cytotoxicity of BC-TA-Mg composites

Calcein-AM staining and CCK-8 assay were conducted to evaluate the potential cytotoxicity of BC-TA-Mg composites on CCC-ESF-1. Fig. 11a exhibits live cells of different groups during the three days' incubation. On day 1, the number of live cells treated with the extracts of BC-TA and BC-TA-2Mg decreased compared with control. In comparison, BC-TA-4Mg and BC-TA-6Mg groups showed almost the same amount

Downloaded from https://academic.oup.com/rb/advance-article/doi/10.1093/rb/rbab054/6381593 by Viikki Science Library user on 07 October 2021

of live cells as control. On day 2, cell number increased for the control, BC-TA-4Mg and BC-TA-6Mg groups, and the control group displayed the most considerable amount of live cells, followed by BC-TA-6Mg, BC-TA-4Mg, BC-TA-2Mg and BC-TA in sequence. The trends almost kept the same on day 3. BC-TA group showed the smallest cell number, and BC-TA-Mg composites revealed lower cytotoxicity on CCC-ESF-1.

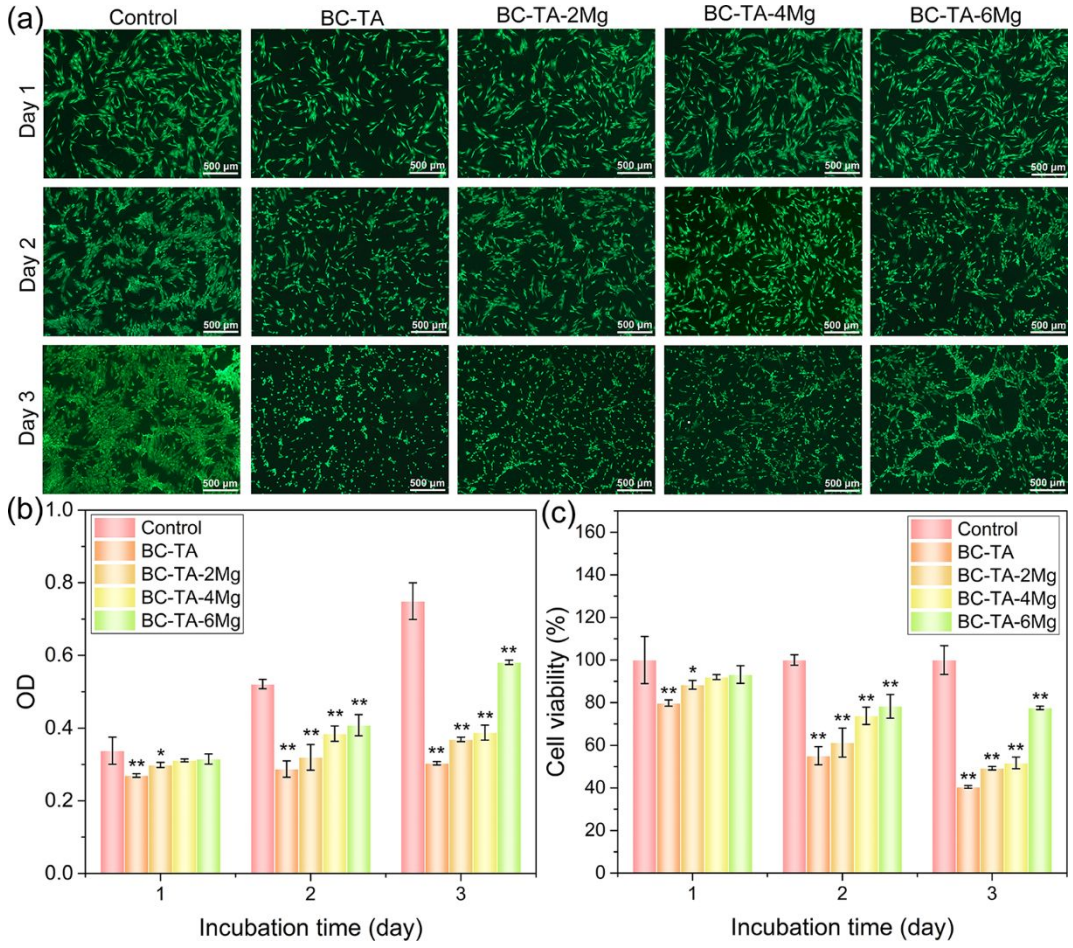

Fig. 11 (a) Calcein-AM staining for live cells. Results of CCK-8 assay: (b) OD values, (c) cell viability. *$p < 0.05$ compared with control group, **$p < 0.01$ compared with control group.

Fig. 11b displays the OD at 450 nm detected by CCK-8 assay, and Fig. 12c depicts cell

Downloaded from https://academic.oup.com/rb/advance-article/doi/10.1093/rb/rbab054/6381593 by Viikki Science Library user on 07 October 2021

viability calculated by normalizing OD to that of the control. On day 1, the treatment of BC-TA and BC-TA-2Mg extracts decreased cell viability to 80 ± 1% and 88 ± 2%, respectively. Treatment with extracts of BC-TA-4Mg and BC-TA-6Mg did not significantly reduce cell viability compared with control. As treatment time prolonged, cell viability decreased for all the experimental groups. Cells treated with BC-TA-6Mg extracts showed a viability of 78 ± 6% and 78 ± 0% on days 2 and 3, respectively, indicating that cells treated with BC-TA-6Mg showed stable cell viability after 2 day's exposure. Supplementary Fig. S2 verified that cells displayed stable viability (77% ± 5%) after treatment with BC-TA-6Mg extracts for 7 days. There was no significant difference between the cell viability of the BC-TA-6Mg group on the tested three timepoints (day 2, 3 and 7).

The above results revealed that the released TA from the membranes displayed a certain degree of cytotoxicity to CCC-ESF-1, and the cytotoxicity of the membranes depended on the concentration of Mg^{2+} incorporated in the BC matrix. Previous studies also showed that the TA incorporated composites decreased viability of 3T3 fibroblast cell lines and murine RAW264.7 macrophage cells after 24 h' or 48 h' exposure [31, 53]. As discussed above, the incorporation of Mg^{2+} contributed to the controlled release of TA. The concentration of released TA decreased as the Mg^{2+} content increased. Therefore, cell viability increased as the Mg^{2+} content increased. On the other hand, BC-TA-Mg composites may also release Mg^{2+}, and the released Mg^{2+} also contributed to improved cell viability as they can serve as a micronutrient for cells [54]. This study indicated that cells treated with the extracts of BC-TA-6Mg composites showed stable

Downloaded from https://academic.oup.com/rb/advance-article/doi/10.1093/rb/rbab054/6381593 by Viikki Science Library user on 07 October 2021

viability of 77%-78% after 2 days' exposure. According to the United States pharmacopeia about toxicity classification, the material was eligible when it showed cell viability of not lower than 75%. The cytotoxicity grade for the material was 0 to 1 [55]. Besides, BC-TA-6Mg showed significant inhibition against the biofilm of singly-cultured *S. aureus*, *P. aeruginosa* and co-cultured *S. aureus* and *P. aeruginosa*, revealing that BC-TA-6Mg composites are potential to be used as wound dressings to deal with biofilms in chronic wounds.

4. Conclusions

In the present study, BC-TA-Mg composite membranes were fabricated by immersing BC in TA and $MgCl_2$ solution in sequence. SEM images showed that TA and $MgCl_2$ particles adhered to the nanofibers of the BC matrix. EPMA results displayed that Mg elements distributed homogeneously across the surface of BC-TA-Mg membranes while no Mg was found on BC and BC-TA membranes. XPS data verified the existence of $MgCl_2$ in the BC-TA-6Mg composite. The surface roughness and hydrophobicity of the membranes increased with the increase of Mg content. Moreover, the introduction of TA and $MgCl_2$ did not influence the transparency of the membranes, making it beneficial for wound inspection. BC-TA and BC-TA-Mg composite membranes displayed significantly increased tensile strength and elongation at break compared to pure BC membranes. BC-TA-Mg exhibited higher water absorption and retention capacity than BC and BC-TA. Furthermore, BC-TA-Mg revealed controlled release of TA depending on the concentration of Mg^{2+}. Gram staining, FITC-ConA staining, and plate counting method showed that BC-TA-Mg composites demonstrated excellent

Downloaded from https://academic.oup.com/rb/advance-article/doi/10.1093/rb/rbab054/6381593 by Viikki Science Library user on 07 October 2021

inhibitory activities on biofilms of singly-cultured *P. aeruginosa*, *S. aureus*, and co-cultured *S. aureus* and *P. aeruginosa*. Live cells staining and CCK-8 assay proved that the cytotoxicity grade of BC-TA-6Mg was eligible. The above outcomes indicated that BC-TA-Mg composites are potential to be used as wound dressings to treat chronic wounds. More broadly, research is also needed to determine TA's anti-biofilm activities, which is fruitful for our further work.

Acknowledgments

This work was financially supported by the National Natural Science Foundation of China (grant numbers 51973018, 51773018, 31700829, and 52063030), Fundamental Research Funds for the Central Universities and the Youth Teacher International Exchange & Growth Program (grant number QNXM20210019), Key Research and Development Projects of People's Liberation Army (grant number BWS17J036), Natural Science Foundation of Jiangxi Province of China (grant number 20192ACB20033).

Conflicts of interest statement: None declared.

References

1. Homaeigohar S, Boccaccini AR. Antibacterial biohybrid nanofibers for wound dressings. *Acta Biomaterialia* 2020;**107**:25-49.

2. Wu Y-K, Cheng N-C, Cheng C-M. Biofilms in Chronic Wounds: Pathogenesis and Diagnosis. *Trends in Biotechnology* 2019;**37**:505-517.

3. Jiang Y, Huang S, Fu X *et al*. Epidemiology of chronic cutaneous wounds in China. *Wound Repair and Regeneration* 2011;**19**:181-188.

Downloaded from https://academic.oup.com/rb/advance-article/doi/10.1093/rb/rbab054/6381593 by Viikki Science Library user on 07 October 2021

4. European commision, https://cordis.europa.eu/article/id/92892-device-for-diabetic-foot-ulcers, 2014.

5. Rondas AALM, Schols JMGA, Stobberingh EE *et al*. Prevalence of chronic wounds and structural quality indicators of chronic wound care in Dutch nursing homes. *International Wound Journal* 2015;**12**:630-635.

6. Hoiby N, Bjarnsholt T, Moser C *et al*. ESCMID* guideline for the diagnosis and treatment of biofilm infections 2014. *Clinical Microbiology and Infection* 2015;**21**:S1-S25.

7. James GA, Swogger E, Wolcott RD *et al*. Biofilms in chronic wounds. *Wound Repair and Regeneration* 2008;**16**:37-44.

8. Malone M, Bjarnsholt T, McBain AJ *et al*. The prevalence of biofilms in chronic wounds: a systematic review and meta-analysis of published data. *J. Wound Care* 2017;**26**:20-25.

9. Kadam S, Shai S, Shahane A *et al*. Recent Advances in Non-Conventional Antimicrobial Approaches for Chronic Wound Biofilms: Have We Found the "Chink in the Armor'? *Biomedicines* 2019;**7**.

10. Bowler PG, Duerden BI, Armstrong DG. Wound microbiology and associated approaches to wound management. *Clinical Microbiology Reviews* 2001;**14**:244-+.

11. Omar A, Wright JB, Schultz G *et al*. Microbial Biofilms and Chronic Wounds. *Microorganisms* 2017;**5**.

12. Metcalf DG, Bowler PG. Clinician perceptions of wound biofilm. *International Wound Journal* 2016;**13**:717-725.

Downloaded from https://academic.oup.com/rb/advance-article/doi/10.1093/rb/rbab054/6381593 by Viikki Science Library user on 07 October 2021

13. Mosselhy DA, Assad M, Sironen T *et al*. Nanotheranostics: A Possible Solution for Drug-Resistant Staphylococcus aureus and their Biofilms? *Nanomaterials* 2021;**11**.

14. Ahmed J, Gultekinoglu M, Edirisinghe M. Bacterial cellulose micro-nano fibres for wound healing applications. *Biotechnology advances* 2020:107549-107549.

15. He W, Wu J, Xu J *et al*. Bacterial Cellulose: Functional Modification and Wound Healing Applications. *Adv. Wound Care*: 10.1089/wound.2020.1219.

16. Picolotto A, Pergher D, Pereira GP *et al*. Bacterial cellulose membrane associated with red propolis as phytomodulator: Improved healing effects in experimental models of diabetes mellitus. *Biomedicine & Pharmacotherapy* 2019;**112**.

17. Liu H, Hu Y, Zhu Y *et al*. A simultaneous grafting/vinyl polymerization process generates a polycationic surface for enhanced antibacterial activity of bacterial cellulose. *International Journal of Biological Macromolecules* 2020;**143**:224-234.

18. Wu J, Zheng Y, Song W *et al*. In situ synthesis of silver-nanoparticles/bacterial cellulose composites for slow-released antimicrobial wound dressing. *Carbohydrate Polymers* 2014;**102**:762-771.

19. Wu J, Zheng Y, Wen X *et al*. Silver nanoparticle/bacterial cellulose gel membranes for antibacterial wound dressing: investigation in vitro and in vivo. *Biomed. Mater.* 2014;**9**:035005.

20. Zhang Z, Sun Y, Zheng Y *et al*. A biocompatible bacterial cellulose/tannic acid composite with antibacterial and anti-biofilm activities for biomedical applications. *Materials Science and Engineering: C* 2020;**106**:110249.

21. Chung K, Wong TY, Wei C *et al*. Tannins and Human Health: A Review. *Critical*

Downloaded from https://academic.oup.com/rb/advance-article/doi/10.1093/rb/rbab054/6381593 by Viikki Science Library user on 07 October 2021

Reviews in Food Science and Nutrition 1998;**38**:421-464.

22. Lee J-H, Park J-H, Cho HS *et al*. Anti-biofilm activities of quercetin and tannic acid against Staphylococcus aureus. *Biofouling* 2013;**29**:491-499.

23. Gjodsbol K, Christensen JJ, Karlsmark T *et al*. Multiple bacterial species reside in chronic wounds: a longitudinal study. *International Wound Journal* 2006;**3**:225-231.

24. Hammond A, Miller KG, Kruczek C *et al*. An in vitro biofilm model to examine the effect of antibiotic ointments on biofilms produced by burn wound bacterial isolates. *Burns* 2011;**37**:312-321.

25. Kucera J, Sojka M, Pavlik V *et al*. Multispecies biofilm in an artificial wound bed—A novel model for in vitro assessment of solid antimicrobial dressings. *Journal of Microbiological Methods* 2014;**103**:18-24.

26. Sun Y, Dowd SE, Smith E *et al*. In vitro multispecies Lubbock chronic wound biofilm model. *Wound Repair and Regeneration* 2008;**16**:805-813.

27. He W, Zhang ZY, Zheng YD *et al*. Preparation of aminoalkyl-grafted bacterial cellulose membranes with improved antimicrobial properties for biomedical applications. *J. Biomed. Mater. Res. Part A* 2020;**108**:1086-1098.

28. Sun Y, Meng C, Zheng Y *et al*. The effects of two biocompatible plasticizers on the performance of dry bacterial cellulose membrane: a comparative study. *Cellulose* 2018;**25**:5893-5908.

29. Seyama H, Soma M. X-ray photoelectron spectroscopic study of montmorillonite containing exchangeable divalent cations. *Journal of the Chemical Society, Faraday Transactions 1: Physical Chemistry in Condensed Phases* 1984;**80**:237-248.

Downloaded from https://academic.oup.com/rb/advance-article/doi/10.1093/rb/rbab054/6381593 by Viikki Science Library user on 07 October 2021

30. He W, Huang X, Zheng Y *et al*. In situ synthesis of bacterial cellulose/copper nanoparticles composite membranes with long-term antibacterial property. *Journal of Biomaterials Science, Polymer Edition* 2018;**29**:2137-2153.

31. Ninan N, Forget A, Shastri VP *et al*. Antibacterial and Anti-Inflammatory pH-Responsive Tannic Acid-Carboxylated Agarose Composite Hydrogels for Wound Healing. *Acs Applied Materials & Interfaces* 2016;**8**:28511-28521.

32. Lee HY, Hwang CH, Kim HE *et al*. Enhancement of bio-stability and mechanical properties of hyaluronic acid hydrogels by tannic acid treatment. *Carbohydrate Polymers* 2018;**186**:290-298.

33. Roman M, Winter WT. Effect of sulfate groups from sulfuric acid hydrolysis on the thermal degradation behavior of bacterial cellulose. *Biomacromolecules* 2004;**5**:1671-1677.

34. Xie Y, Zheng Y, Fan J *et al*. Novel Electronic-Ionic Hybrid Conductive Composites for Multifunctional Flexible Bioelectrode Based on in Situ Synthesis of Poly(dopamine) on Bacterial Cellulose. *Acs Applied Materials & Interfaces* 2018;**10**:22692-22702.

35. de Souza CF, Lucyszyn N, Woehl MA *et al*. Property evaluations of dry-cast reconstituted bacterial cellulose/tamarind xyloglucan biocomposites. *Carbohydrate Polymers* 2013;**93**:144-153.

36. Palmer KL, Mashburn LM, Singh PK *et al*. Cystic Fibrosis Sputum Supports Growth and Cues Key Aspects of Pseudomonas aeruginosa Physiology. *Journal of Bacteriology* 2005;**187**:5267-5277.

37. Palmer KL, Aye LM, Whiteley M. Nutritional Cues Control Pseudomonas aeruginosa

Downloaded from https://academic.oup.com/rb/advance-article/doi/10.1093/rb/rbab054/6381593 by Viikki Science Library user on 07 October 2021

Multicellular Behavior in Cystic Fibrosis Sputum. *Journal of Bacteriology* 2007;**189**:8079-8087.

38. Deleon S, Clinton A, Fowler H *et al*. Synergistic Interactions of Pseudomonas aeruginosa and Staphylococcus aureus in an In Vitro Wound Model. *Infection and Immunity* 2014;**82**:4718-4728.

39. Hotterbeekx A, Kumarsingh S, Goossens H *et al*. In vivo and In vitro Interactions between Pseudomonas aeruginosa and Staphylococcus spp. *Frontiers in Cellular and Infection Microbiology* 2017;**7**:106-106.

40. Zajdel M, Wagrzynowicz Z, Jeljaszewicz J. Action of staphylothrombin on bovine fibrinogen. *Thrombosis Research* 1975;**6**:501-510.

41. Ozyurek SB, Gur SD, Bilkay IS. Production of pyocyanin pigment from Pseudomonas aeruginosa strains and investigation of the antimicrobial effect of pyocyanin on other microorganisms. *Current Opinion in Biotechnology* 2011;**22**:S113-S113.

42. Jayaseelan S, Ramaswamy D, Dharmaraj S. Pyocyanin: production, applications, challenges and new insights. *World Journal of Microbiology & Biotechnology* 2014;**30**:1159-1168.

43. Colak SM, Yapici BM, Yapici AN. Determination of antimicrobial activity of tannic acid in pickling process. *Romanian Biotechnological Letters* 2010;**15**:5325-5330.

44. Akiyama H, Fujii K, Yamasaki O *et al*. Antibacterial action of several tannins against Staphylococcus aureus. *Journal of Antimicrobial Chemotherapy* 2001;**48**:487-491.

45. Chung KT, Lu Z, Chou MW. Mechanism of inhibition of tannic acid and related compounds on the growth of intestinal bacteria. *Food and chemical toxicology : an*

Downloaded from https://academic.oup.com/rb/advance-article/doi/10.1093/rb/rbab054/6381593 by Viikki Science Library user on 07 October 2021

international journal published for the British Industrial Biological Research Association 1998;**36**:1053-1060.

46. Payne DE, Martin NR, Parzych KR *et al*. Tannic Acid Inhibits Staphylococcus aureus Surface Colonization in an IsaA-Dependent Manner. *Infection and Immunity* 2013;**81**:496-504.

47. Cho HS, Lee JH, Ryu SY *et al*. Inhibition of Pseudomonas aeruginosa and Escherichia coli O157:H7 Biofilm Formation by Plant Metabolite epsilon-Viniferin. *J. Agric. Food Chem.* 2013;**61**:7120-7126.

48. Siddiqui MF, Rzechowicz M, Oh HS *et al*. The efficacy of tannic acid in controlling biofouling by Pseudomonas aeruginosa is dependent on nutrient conditions and bacterial density. *Int. Biodeterior. Biodegrad.* 2015;**104**:74-82.

49. Chusri S, Phatthalung PN, Voravuthikunchai SP. Anti-biofilm activity of Quercus infectoria G. Olivier against methicillin-resistant Staphylococcus aureus. *Lett. Appl. Microbiol.* 2012;**54**:511-517.

50. Sarabhai S, Sharma P, Capalash N. Ellagic Acid Derivatives from Terminalia chebula Retz. Downregulate the Expression of Quorum Sensing Genes to Attenuate Pseudomonas aeruginosa PAO1 Virulence. *Plos One* 2013;**8**.

51. Siddiqui MF, Oh H-S, Rzechowicz M *et al*. Biofouling control potential of tannic acid, ellagic acid, and epigallocatechin against Pseudomonas aeruginosa and reverse osmosis membrane multispecies community. *Journal of Industrial and Engineering Chemistry* 2015;**30**:204-211.

52. Chang C, Krishnan T, Wang H *et al*. Non-antibiotic quorum sensing inhibitors acting

Downloaded from https://academic.oup.com/rb/advance-article/doi/10.1093/rb/rbab054/6381593 by Viikki Science Library user on 07 October 2021

against N-acyl homoserine lactone synthase as druggable target. *Scientific Reports* 2015;**4**:7245-7245.

53. Lomova MV, Brichkina AI, Kiryukhin MV *et al*. Multilayer Capsules of Bovine Serum Albumin and Tannic Acid for Controlled Release by Enzymatic Degradation. *Acs Applied Materials & Interfaces* 2015;**7**:11732-11740.

54. Huang Q, Li X, Liu T *et al*. Enhanced SaOS-2 cell adhesion, proliferation and differentiation on Mg-incorporated micro/nano-topographical TiO2 coatings. *Applied Surface Science* 2018;**447**:767-776.

55. USP XXII, [S] NX. Toxicity classification in US Pharmacopeia. *United States Pharmacopeial Convention, Inc.* 2018:2069.

Downloaded from https://academic.oup.com/rb/advance-article/doi/10.1093/rb/rbab054/6381593 by Viikki Science Library user on 07 October 2021

Supplementary data

Materials and Methods

2.1 SEM observation

To check whether the bacteria or biofilm adhered on and penetrated BC-TA and BC-TA-Mg composites during the experiments, the composites after removal from the artificial wound bed were collected for SEM observation. Briefly, the material was rinsed twice with PBS and then fixed in 2.5% glutaraldehyde. Afterward, it was immersed in a series of graded ethanol (30, 50, 75, 85, 95, and 100 v/v%) for dehydration. After that, the membrane was treated with a series of tertiary butyl alcohol (25, 50, 75, and 100 v/v%) for solvent replacement. At last, it was freeze-dried, sputtered with platinum, and then observed by SEM (GeminiSEM 300, ZEISS, Germany).

Supplementary Figure 1

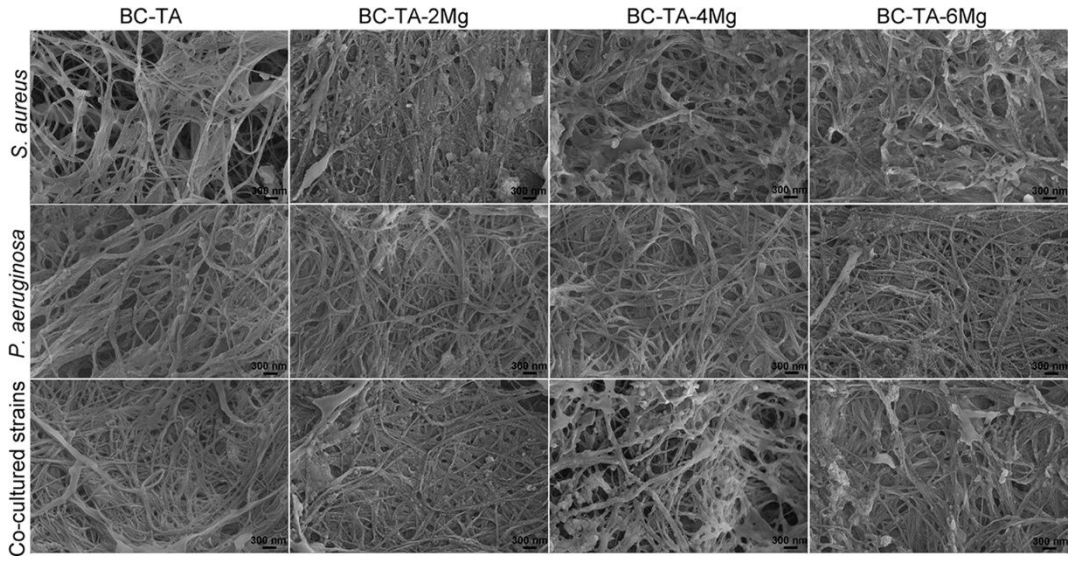

Fig. S1 SEM images of BC-TA and BC-TA-Mg composites removed from the biofilm

Downloaded from https://academic.oup.com/rb/advance-article/doi/10.1093/rb/rbab054/6381593 by Viikki Science Library user on 07 October 2021

of singly-cultured *S. aureus*, *P. aeruginosa,* and co-cultured *S. aureus* and *P. aeruginosa*.

Supplementary Figure 2

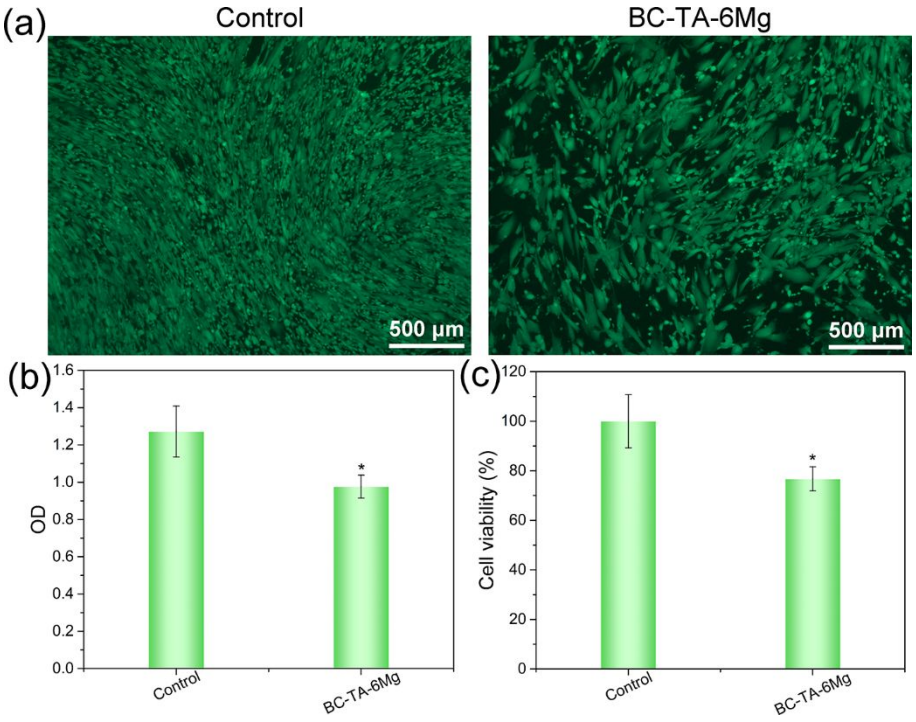

Fig. S2 (a) Calcein-AM staining for live cells. Results of CCK-8 assay: (b) OD values, (c) cell viability. *$p < 0.05$ compared with control group.

Downloaded from https://academic.oup.com/rb/advance-article/doi/10.1093/rb/rbab054/6381593 by Viikki Science Library user on 07 October 2021

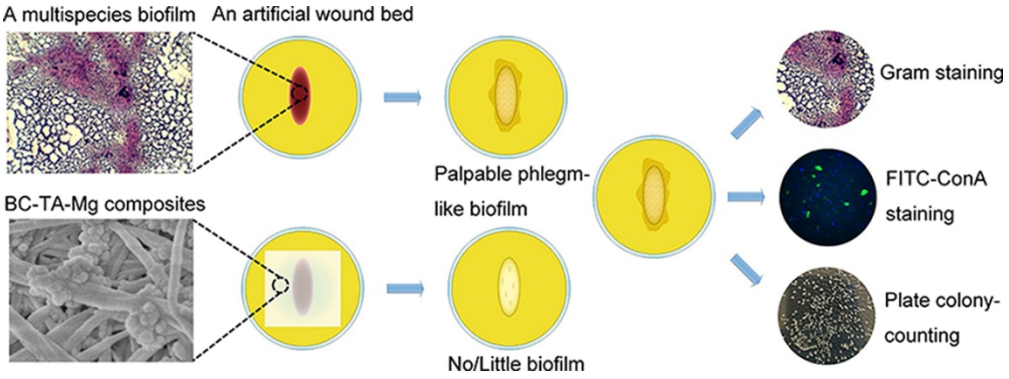

Fig. 1 Schematic illustration of the anti-biofilm activities of BC-TA-Mg composites and the related tests performed in this study.

Downloaded from https://academic.oup.com/rb/advance-article/doi/10.1093/rb/rbab054/6381593 by Viikki Science Library user on 07 October 2021

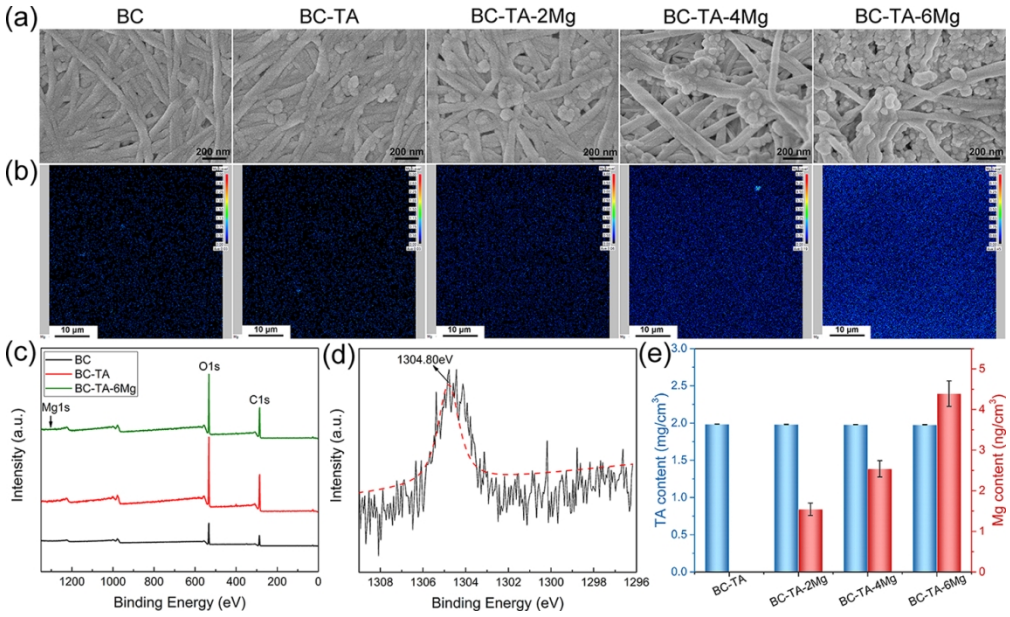

Fig. 2 SEM images (a) and Mg elements distribution detected by EPMA (b) of BC, BC-TA, BC-TA-2Mg, BC-TA-4Mg, and BC-TA-6Mg membranes. (c) XPS survey spectra of BC, BC-TA, and BC-TA-6Mg membranes. (d) High-resolution XPS spectra of Mg 1s. (e) The content of TA and Mg in different samples.

Downloaded from https://academic.oup.com/rb/advance-article/doi/10.1093/rb/rbab054/6381593 by Viikki Science Library user on 07 October 2021

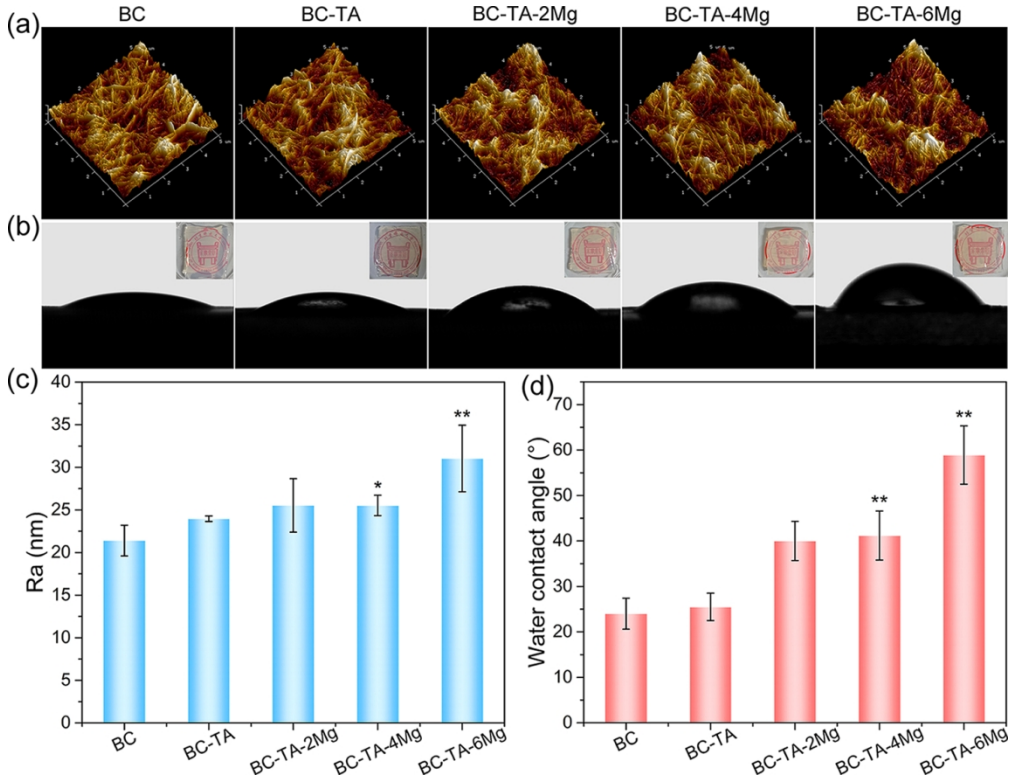

Fig. 3 AFM images (a) and water contact angles images (b) of BC, BC-TA, BC-TA-2Mg, BC-TA-4Mg, and BC-TA-6Mg membranes. The inserted pictures in (b) were the photographs of five membranes. The histogram of Ra (c) and water contact angle (d) of different samples. *p < 0.05 compared with BC group, **p < 0.01 compared with BC group.

Downloaded from https://academic.oup.com/rb/advance-article/doi/10.1093/rb/rbab054/6381593 by Viikki Science Library user on 07 October 2021

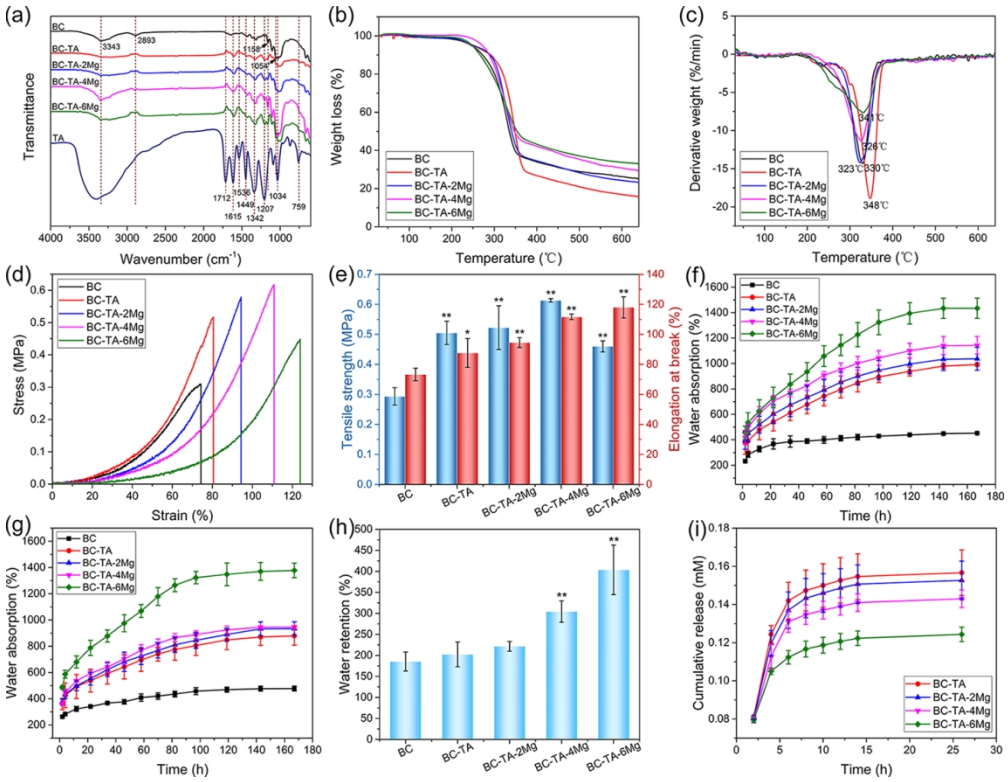

Fig. 4 (a) FTIR spectrum of BC, BC-TA, BC-TA-2Mg, BC-TA-4Mg, and BC-TA-6Mg membranes. Weight loss (b) and derivative weight (c) of different samples. Tensile stress-strain curves (d) and histogram of tensile strength and elongation at break (e) of different samples. Water absorption capacity of different samples at pH 5 (f) and pH 8 (g). (h) Water retention rate of different samples. (i) In vitro release curve of TA from BC-TA and BC-TA-Mg composites. *p < 0.05 compared with BC group, **p < 0.01 compared with BC group.

Downloaded from https://academic.oup.com/rb/advance-article/doi/10.1093/rb/rbab054/6381593 by Viikki Science Library user on 07 October 2021

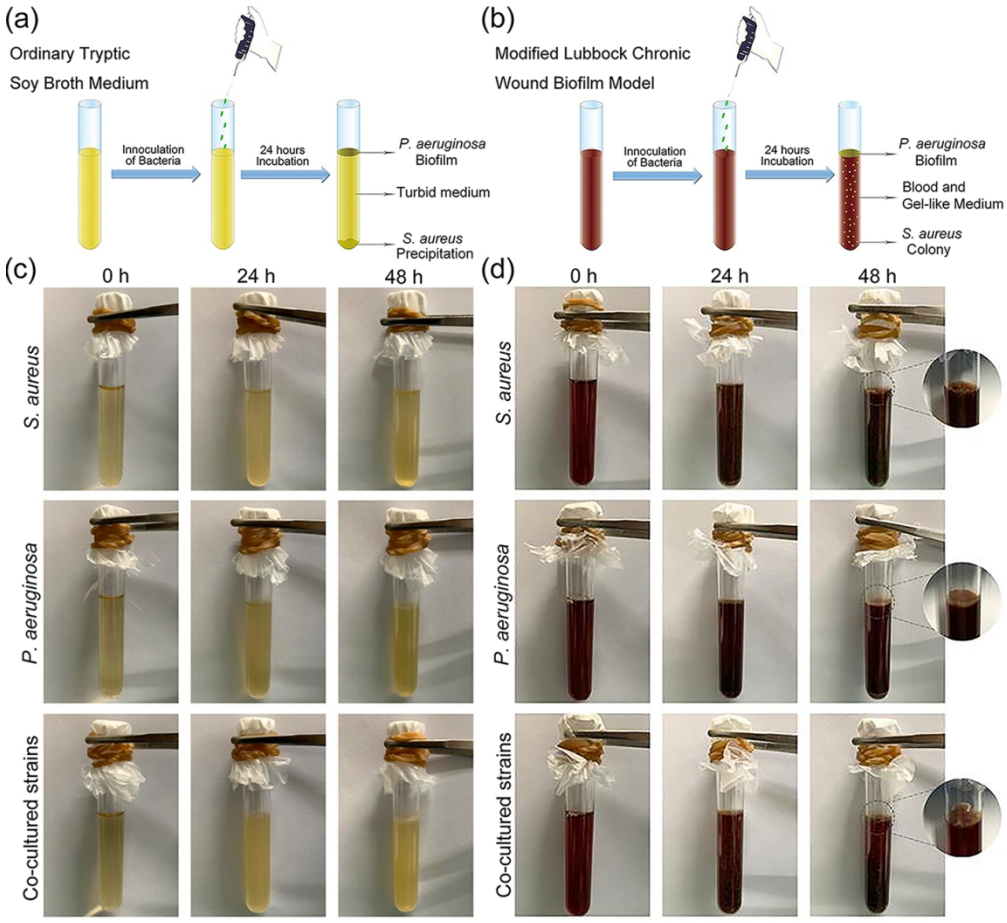

Fig. 5 Schematic illustration for the establishment method of multispecies biofilm model in vitro: bacteria were incubated in ordinary tryptic soy broth medium (a) and modified medium (b). The formation of chronic wound biofilms in vitro: bacteria were incubated in ordinary tryptic soy broth medium (c) and modified medium (d).

Downloaded from https://academic.oup.com/rb/advance-article/doi/10.1093/rb/rbab054/6381593 by Viikki Science Library user on 07 October 2021

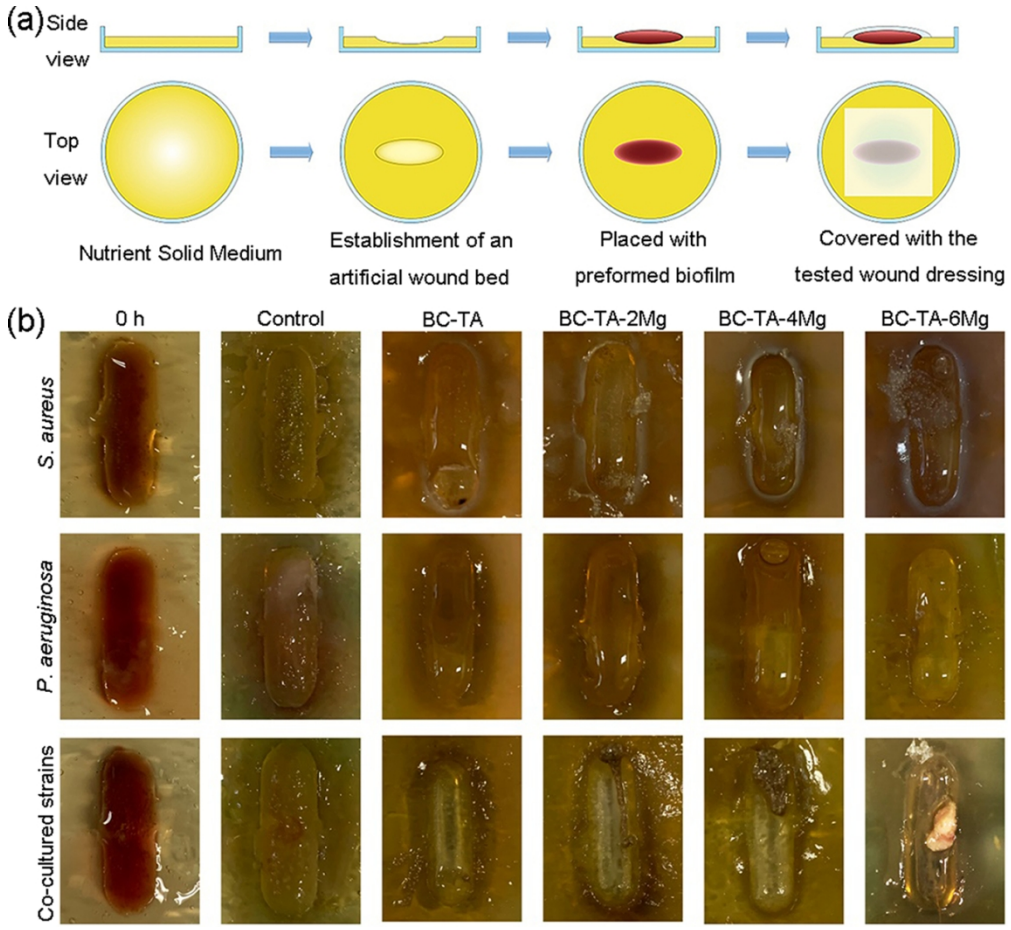

Fig. 6 (a) Schematic illustration for the establishment of biofilm on the artificial wound bed. (b) Photographs of biofilms on artificial wound bed before and after treatment with BC-TA-Mg composites for 24 h.

Downloaded from https://academic.oup.com/rb/advance-article/doi/10.1093/rb/rbab054/6381593 by Viikki Science Library user on 07 October 2021

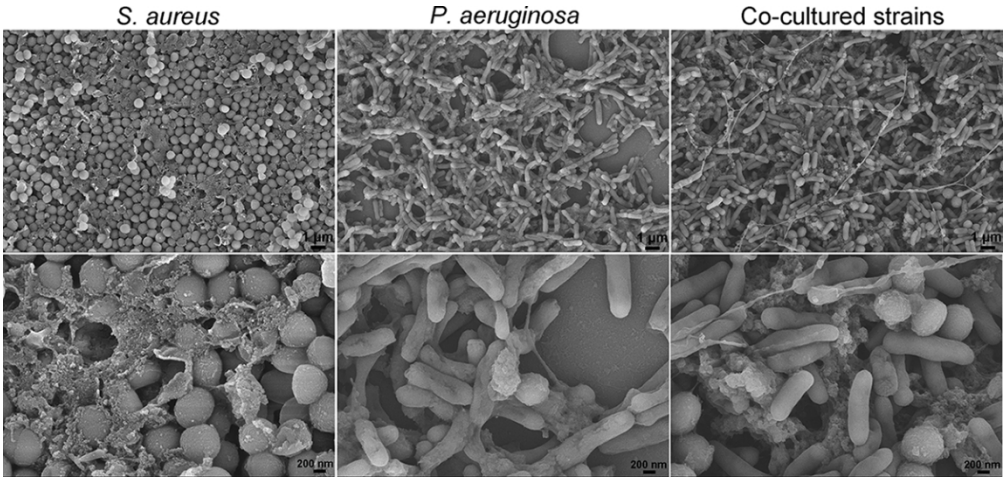

Fig. 7 SEM images of the biofilm model of singly-cultured S. aureus, P. aeruginosa, and co-cultured S. aureus and P. aeruginosa. The images were taken at two different magnifications of 5000× and 20000×.

Downloaded from https://academic.oup.com/rb/advance-article/doi/10.1093/rb/rbab054/6381593 by Viikki Science Library user on 07 October 2021

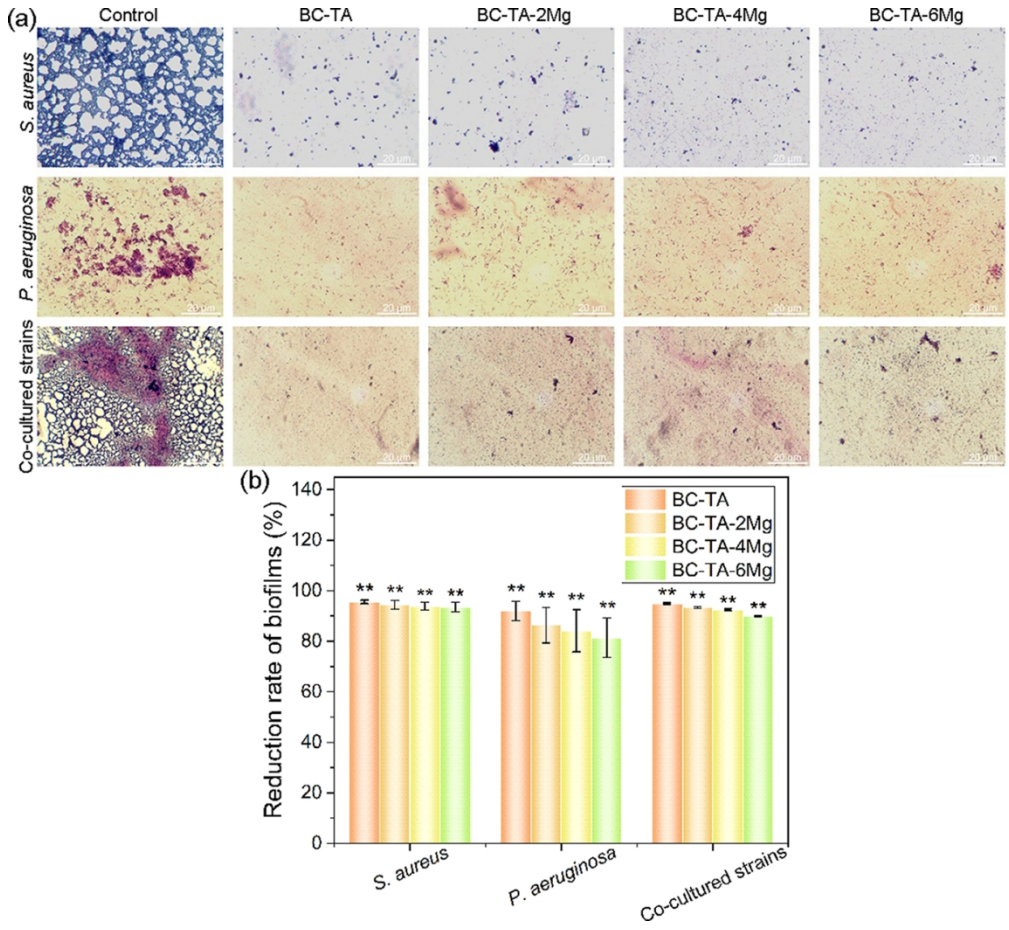

Fig. 8 (a) Gram staining for bacterial biofilm treated with different membranes for 24 h. (b) The quantified reduction rate of stained area based on image data using the software Image-Pro Plus Vision 6.0. **p < 0.01 compared with the control group.

Downloaded from https://academic.oup.com/rb/advance-article/doi/10.1093/rb/rbab054/6381593 by Viikki Science Library user on 07 October 2021

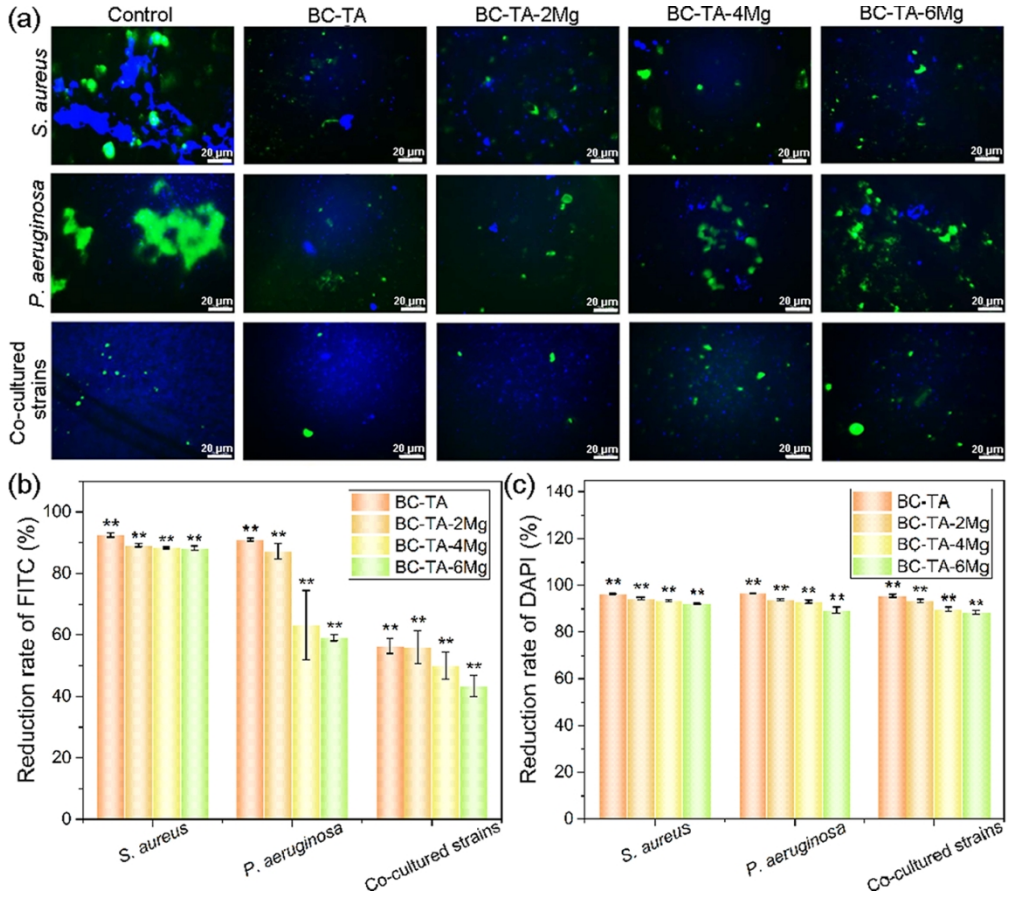

Fig. 9 (a) FITC-ConA and DAPI staining for exopolysaccharides and cell nucleus of bacteria treated with different membranes for 24 h. The quantified reduction rate of intergraded optical density of FITC (b) and DAPI (c) based on image data using the software Image-Pro Plus Vision 6.0. **p < 0.01 compared with control group.

Downloaded from https://academic.oup.com/rb/advance-article/doi/10.1093/rb/rbab054/6381593 by Viikki Science Library user on 07 October 2021

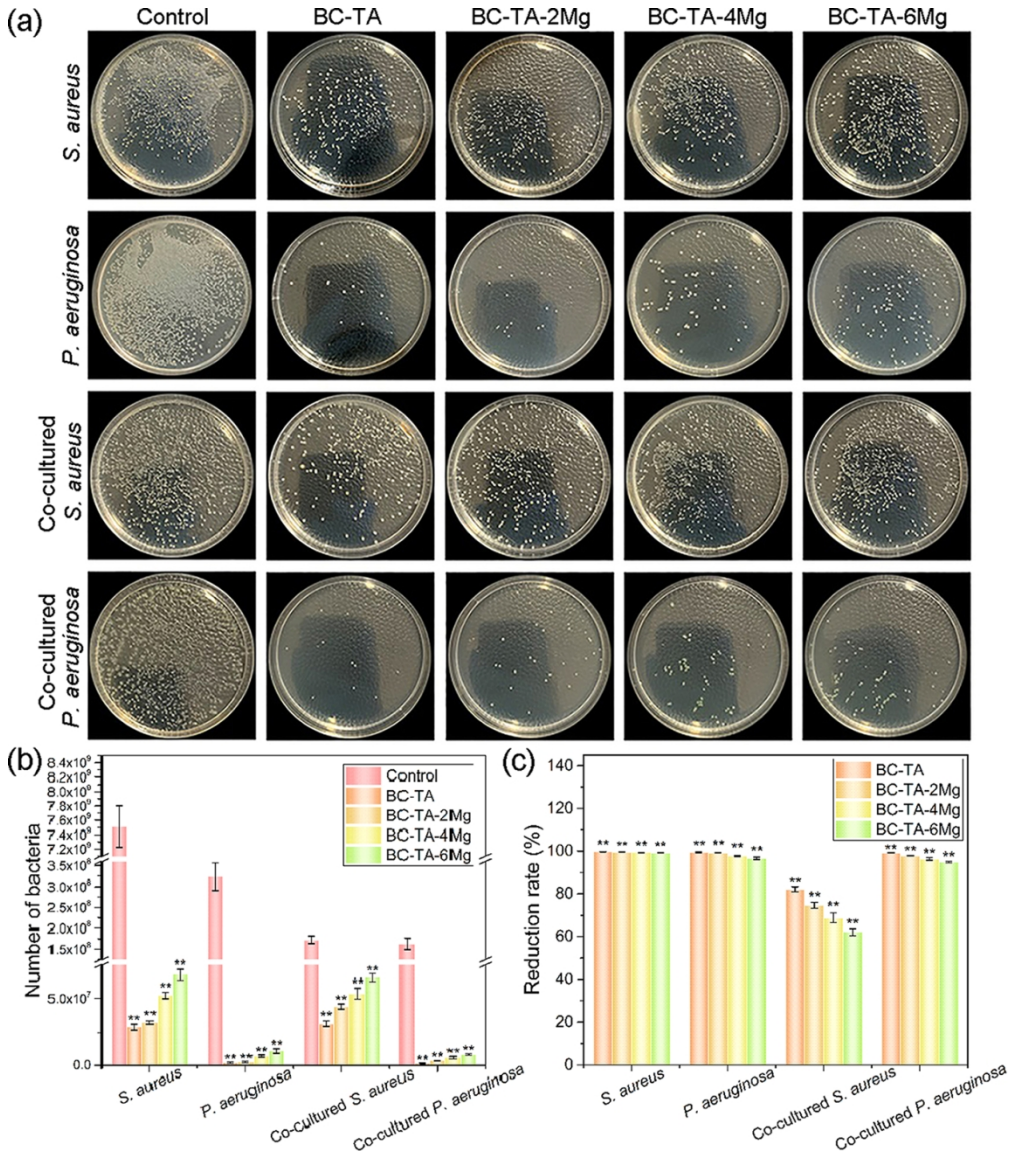

Fig. 10 (a) Photographs of recultivated S. aureus and P. aeruginosa on agar from singly-cultured biofilm or co-cultured biofilm treated with different membranes for 24 h. Number (b) and reduction rate (c) of bacteria from singly-cultured biofilm or co-cultured biofilms treated with different membranes for 24 h. **p < 0.01 compared with control group.

Downloaded from https://academic.oup.com/rb/advance-article/doi/10.1093/rb/rbab054/6381593 by Viikki Science Library user on 07 October 2021

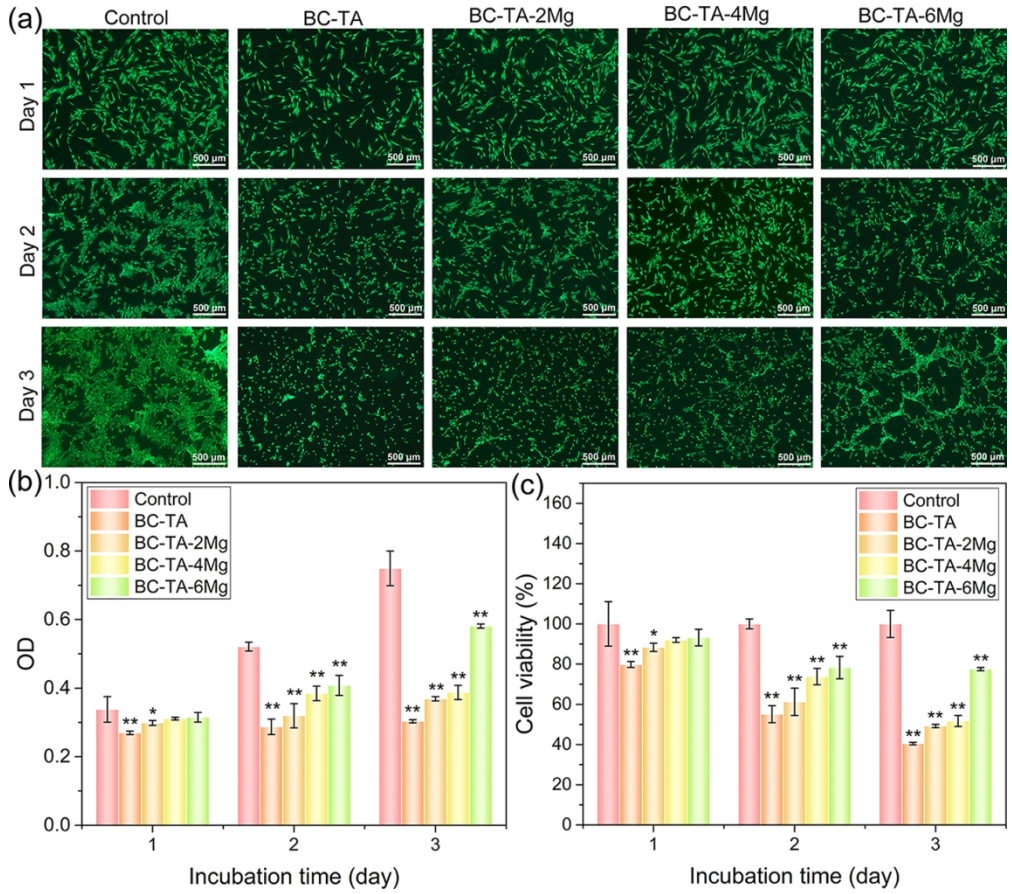

Fig. 11 (a) Calcein-AM staining for live cells. Results of CCK-8 assay: (b) OD values, (c) cell viability. *p < 0.05 compared with control group, **p < 0.01 compared with control group.

Downloaded from https://academic.oup.com/rb/advance-article/doi/10.1093/rb/rbab054/6381593 by Viikki Science Library user on 07 October 2021